

UNIVERSIDAD SAN FRANCISCO DE QUITO USFQ

Colegio de Ciencias e Ingenierías

**Analysis of hyperbolic metamaterials using the
differential method**

Proyecto de investigación

Jorge Luis Campos Pazmiño

Licenciatura en Física

Trabajo de titulación presentado como requisito
para la obtención del título de Licenciado en Física

Quito, 24 de mayo de 2018

UNIVERSIDAD SAN FRANCISCO DE QUITO USFQ
COLEGIO DE CIENCIAS E INGENIERÍAS

**HOJA DE CALIFICACIÓN
DE TRABAJO DE TITULACIÓN**

**Analysis of hyperbolic metamaterials using the
differential method**

Jorge Luis Campos Pazmiño

Calificación:

Nombre del profesor: Melissa Infusino Ph.D.

Firma del profesor: _____

Quito, 24 de mayo de 2018

DERECHOS DE AUTOR

Por medio del presente documento certifico que he leído todas las Políticas y Manuales de la Universidad San Francisco de Quito USFQ, incluyendo la Política de Propiedad Intelectual USFQ, y estoy de acuerdo con su contenido, por lo que los derechos de propiedad intelectual del presente trabajo quedan sujetos a lo dispuesto en esas Políticas.

Asimismo, autorizo a la USFQ para que realice la digitalización y publicación de este trabajo en el repositorio virtual, de conformidad a lo dispuesto en el Art. 144 de la Ley Orgánica de Educación Superior.

Firma del estudiante: -----

Nombres y apellidos: Jorge Luis Campos Pazmiño

Código: 00110951

Cédula de identidad: 1003158746

Lugar y fecha: Quito, 24 de mayo de 2018

A mis padres y hermano.

Agradecimientos

Este trabajo representa el final de un largo viaje, hermoso e incluso, muy difícil en ocasiones. Junto a mí, en este viaje siempre estuvieron mis padres y mi hermano. Para ellos, todo lo que tengo y tendré para ofrecer.

Me gustaría agradecer de manera muy especial a Melissa Infusino y Alessandro Veltri.

Dos personas, que más allá de ser excelentes profesores y físicos, su verdadero valor radica en los increíbles seres humanos que moldearon mi forma de pensar en el ámbito profesional y humano. También me encantaría agradecer a Demetrio Macias, profesor de la Université de Technologie de Troyes, quien fue el responsable de dar inicio a este proyecto.

Finalmente, no puedo olvidar a todas las personas especiales que conocí durante el viaje. Gracias a todos mis amigos y colegas.

Jorge Campos Quito, 2 de diciembre del 2017.

Resumen

En el presente trabajo se analizará metamateriales hiperbólicos empleando el método diferencial. En primer lugar, se desarrolla la teoría detrás del método diferencial. Este método sirve para describir los campos eléctricos y magnéticos difractados por una estructura de cualquier geometría y material. Para este trabajo se consideran únicamente estructuras invariantes en una dirección espacial. Después, se explica el desarrollo de un código en lenguaje C++ basado en el método diferencial para describir los campos difractados a través de la matriz de scattering de la estructura considerada. Finalmente, se emplea el código para analizar metamateriales hiperbólicos.

Key words: método diferencial, difracción, metamaterial, metamaterial hiperbólico.

Abstract

In this work hyperbolic metamaterials will be analyzed using the differential method. The first part is dedicated to the theoretical development of the differential method. This method is used to describe the electric and magnetic fields diffracted by a structure of any geometry or material. This particular work will be limited to structures which geometry is invariant along one spatial direction. Then, the development of a code in C++ language based on the differential method is explained. The code is used to describe the diffracted fields in terms of the scattering matrix of the structure. Finally, this code is utilized to analyzed hyperbolic metamaterials.

Key words: differential method, diffraction, hyperbolic metamaterial.

Index

1	Introduction	12
1.1	Spectral methods for light diffraction analysis	12
1.1.1	Classic differential method	12
1.2	Metamaterials	13
1.2.1	What is a metamaterial?	13
1.2.2	Hyperbolic metamaterials and its applications	14
1.3	Aim	15
2	Classic differential method	16
2.1	Definition of the problem	16
2.2	Maxwell equations for TE and TM polarizations	17
2.3	Classic differential method for TE polarization	18
2.3.1	Field equations inside the modulated zone	18
2.3.2	Field equations outside the modulated zone	20
2.4	Classic differential method for TM polarization	22
2.4.1	Field equation	22
2.4.2	Definition of the normal and tangential components at the surface for the electric field	23
2.4.3	L. Li factorization rules	24
2.4.4	Field equations inside the modulated zone	24
2.4.5	Field equations outside the modulated zone	26
2.5	Resolution of the systems of equations for TE and TM polarizations	28
3	Development of a computational tool for the implementation of the differential method and validation of the code	30
3.1	S -matrix propagation algorithm	30
3.2	Runge-Kutta method for the solution of a systems of equations	32
3.3	Code validation	34
3.3.1	Energy conservation	34
3.3.2	Comparison with Fresnel equations	35
3.3.3	Comparison with transmission matrix method	37
4	Applications of the differential method, results and discussion	39
4.1	Propagation of waves in anisotropic media and hyperbolic metamaterials	39
4.1.1	Wave propagation	39
4.1.2	Propagation in an uniaxial media	40
4.1.3	Hyperbolic metamaterials	41
4.2	Analysis of metamaterial using the differential method	45

	9
5 Conclusions	49
Appendices	50
6 References	53

Figure Index

1	Possible properties of an isotropic and lossless material in the ϵ - μ domain [8].	14
2	a) HMM made of alternating layers of dielectric and metal. b) HMM made of metallic nanowires inside a dielectric host.	15
3	Cartesian coordinate system used to describe a structure invariant along one dimension	16
4	Decomposition of the electric field in normal and tangential components	23
5	Representation of the division in layers of the modulated zone and definitions of transmission and scattering matrices	31
6	a) Behavior of the reflectance and transmittance coefficients of a slab of air (index of refraction $\nu = 1$) of height 100 [nm], divided in 10 layers and for which 10 Runge-Kunta steps were considered. Angle of incidence $\theta_i = 0$. b) Behavior of the reflectance and transmittance coefficients of a slab of dielectric (index of refraction $\nu = 4$) of height 100 [nm], divided in 10 layers and for which 10 Runge-Kunta steps were considered. Angle of incidence $\theta_i = 0$	34
7	Reflectance and transmittance coefficients of a gold slab of height 100 [nm] divided in 10 layers and for 10 Runge-Kutta steps and an angle of incidence of 0° . a) Reflectance. b) Transmittance.	35
8	Reflectance and transmittance coefficients of a gold slab of height 100 [nm] divided in 10 layers and 10 Runge-Kunta steps and an angle of incidence of 30° . a) Reflectance for TE polarization. b) Transmittance for TE polarization. c) Reflectance for TM polarization. d) Transmittance for TM polarization.	36
9	Reflectance and transmittance coefficients of a gold slab of height 100 [nm] divided in 10 layers and for 10 Runge-Kunta steps and an angle of incidence of 0° . a) and b) Reflectance and transmittance when the substrate is made of glass ($\nu = 1.5$, layer of 50 [nm]). c) and d) Reflectance and transmittance when the substrate is made of glass ($\nu = 1.5$, layer of 50 [nm]) and the superstrate is made of water ($\nu = 1.5$, layer of 50 [nm]).	38
10	a) Normal surface for an extraordinary wave for a hyperbolic metamaterial. b) Example of a hyporbolic metamaterial made of layers of metal and dielectric materials [25].	41
11	Effective permittivities of a multilayered system made of bilayers of Au (16 [nm] of thickness) and Al_2O_3 (30 [nm] of thickness).	42
12	Effective permittivities of a multilayered system mad of bilayers of Au (16 [nm] of thickness) and TiO_2 (30 [nm] of thickness).	43

13	a) and b) effective permittivities of a multilayered system made of bilayers of silver (10 [nm] of thickness) and TiO_2 (10 [nm] of thickness). c) and d) effective permittivities of a multilayered system made of bilayers of silver (16 [nm] of thickness) and TiO_2 (30 [nm] of thickness).	44
14	Behavior of a HMM made of Ag and TiO_2 depending on the filling factor of the metal layer	45
15	Reflectance and transmittance for a multilayered system of 8 bilayers made of Au (16 [nm]) and Al_2O_3 (30 [nm]), angle of incidence 0°	46
16	Reflectance and transmittance for a multilayered system of 8 bilayers made of Au (16 [nm]) and TiO_2 (30 [nm]), angle of incidence 0°	46
17	Reflectance and transmittance for a multilayered system of 8 bilayers made of Ag (16 [nm]) and TiO_2 (30 [nm]), angle of incidence 0°	47
18	HMM and grating. The HMM is made of 8 bilayers made of Ag (16 [nm]) and TiO_2 (30 [nm]). The HMM and the grating are separated by a layer of 10 [nm] of TiO_2 . The grating is made of PMMA (height of 100 [nm] and length of 160 [nm]) covered by 20 [nm] of Ag. The grating period corresponds to 500 [nm]	48
19	Effect of a grating in a HMM. a) Reflectance of the HMM (8 bilayers of Ag of 16 [nm] and TiO_2 of 30 [nm]). b) Reflectance of the grating of PMMA an Ag. c) Reflecta of the HMM combined with the grating. For all the spectra the angle of incidence was 50°	48
20	Effect of aliasing in a Fourier transform. a) Function $h(t)$ defined for an interval T (the period of the function) and discretize through intervals of length Δ . b) Fourier transform $H(f)$ of the the function $h(t)$. c) Comparison of the real Fourier transform and the aliased transform inside the region defined by the Nyquist critical frequency $f_c = 1/2\Delta$.	51

1 Introduction

1.1 Spectral methods for light diffraction analysis

When light interacts with an object two different phenomena can occur: scattering and absorption of photons. Light keeps information of the object with which it interacts. This information can be “read” through parameters like the intensity, polarization, phase, etc.

Diffraction is a particular form of scattering. The difference between both terms is pretty subtle and many times both are used as synonyms. Scattering is often associated with interactions between small randomly distributed particles and electromagnetic waves. Meanwhile, diffraction is related to interactions that involved organized structures [38].

So, the study of light diffracted by a structure is important due to the fact that different properties of the structure can be known. There are several tools (theoretical and computational) useful to analyze diffracted light. An especial set of these tools are known as “spectral methods”. In general terms, a spectral method consists in a formulation to solve differential equations through a spacial discretization. It gives an approximate solution by a linear combination of suitable trial basis functions. Here the use of test functions ensures that the differential equation and boundary conditions are satisfied by the proposed solution [6]. When spectral methods are used for the analysis of light diffraction, the functions used as basis for the solution of differential equations are generally Fourier series. But, it is extremely important to highlight that Fourier series are just an option among others. Sometimes, boundary conditions appears as Floquet or quasi-periodic functions. Then, the solutions of the differential equations can appear, for example, expressed as a Fourier series modulated by a single plane wave [1].

Some examples of spectral methods for the analysis of light diffraction are: the Rigorous Wave Coupled Wave (RCW) method also known as Fourier modal theory, the integral method, the coordinate transformation methods and the differential method [1].

1.1.1 Classic differential method

The first works involving the differential method appeared during the 1960s. In this works, the method was used for modeling the diffusion of particles in nuclear potentials and it was referred as the “optical method” due to the similarity of the Schrodinger and Helmholtz equations. Later, in 1969 it was used for the description of diffraction gratings. But, the results obtained using the differential method were inaccurate, especially for TM polarization. The numerical problems were eliminated with the subsequent inclusion of the S -matrix propagation algorithm and L. Li factorization rules [1, 19, 26].

1.2 Metamaterials

1.2.1 What is a metamaterial?

The interactions between electromagnetic waves and objects can produce a vastly diverse set of phenomena and allows the functioning of many devices. The response of an object is strongly dependent on elements like its geometry and the materials of fabrication. Although, there are some constraints impossible to overcome, for example that any medium permits a group velocity greater than the speed of light in vacuum, many electromagnetic phenomena and properties can be achieved and are only limited by these two factors.

It is possible to fabricate materials with electromagnetic properties that are not present in nature. These artificial structures engineered to possess some novel electromagnetic properties or to produce a specific phenomenon are called “metamaterials” [7].

The prefix “meta” means “beyond”, thus the word “metamaterials” refers to materials beyond those present in nature. This term was used for the first time in 1999 by Walser, R., a physics professor at the University of Texas for referring to “Macroscopic composites having a synthetic, three dimensional, periodic cellular architecture designed to produce an optimized combination, not available in nature, of two or more responses” [37]. Later the term was used in 2000 by Smith et al. in a paper related to materials with simultaneous negative permittivity and permeability. This type of materials are called double negative materials (DNG) or left-handed materials (LHM) [8]. Interestingly, LHM were previously described theoretically by Veselago in 1968 [8]. But, they did not attract the scientific community during 30 years due to lack of experimental verification or the presence of such characteristic in nature [37].

Nowadays, the term “metamaterial” is not limited only to LHM. Usually a material is characterized by its permittivity (ϵ) and permeability (μ). In Figure 1 are shown all possible properties of isotropic and lossless materials depending on the values of ϵ and μ . The first quadrant ($\epsilon > 0$ and $\mu > 0$) represents right-handed materials (RHM). The second ($\epsilon < 0$ and $\mu > 0$), corresponds to electric plasma that supports evanescent waves. The third quadrant ($\epsilon < 0$ and $\mu < 0$) are LHM. Finally, the fourth quadrant ($\epsilon > 0$ and $\mu < 0$) represents magnetic plasma that supports evanescent waves.

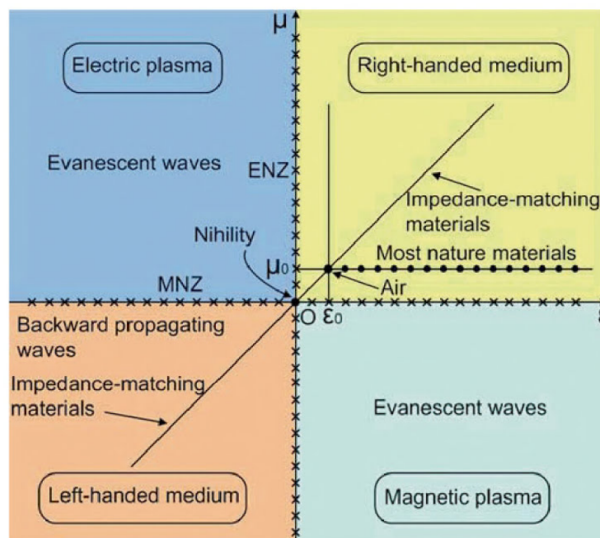


Figure 1: Possible properties of an isotropic and lossless material in the ϵ - μ domain [8].

In Figure 1 other metamaterials with different properties can be observed. For μ_0 and ϵ_0 the permeability and permittivity of vacuum, respectively. There are metamaterials that presents $\mu = -\mu_0$ and $\epsilon = -\epsilon_0$. It is a LHM that has “anti-air” properties producing a perfect lens. The line $\epsilon = \mu$ represents metamaterials that have perfect impedance matching with air, resulting in no reflections. There are some materials with $\epsilon = 0$ (ϵ -near zero -ENZ-) and $\mu = 0$ (μ -near zero -MNZ-) with special properties. Finally, in the first quadrant, only exist certain discrete points with $\mu = \mu_0$ and $\epsilon \geq \epsilon_0$ which represent most of the natural materials that exist. Thus, even for RHM some properties are only obtained by metamaterials [8].

One approach to construct a metamaterial is to create a structure made of well-arranged elements of subwavelength dimensions. Although this building blocks are several orders beyond the atomic or molecular level, these are still considerably smaller than wavelengths of interest and their electromagnetic responses can be expressed in terms of homogenized “effective” parameters [7].

1.2.2 Hyperbolic metamaterials and its applications

Hyperbolic metamaterials (HMM) are a particular set of metamaterials first introduced to overcome the diffraction limit of optical imaging. With time, many other applications that involved these metamaterials were considered. For example: hyper lenses, perfect nanolenses, invisibility cloaks, enhanced quantum-electrodynamics effects, thermal hyperconductivity and even gravitation theory analogues [5, 32].

A HMM is an uniaxial material that possesses dielectric properties in one direction and metallic properties in an orthogonal direction. This kind of behavior, at optical

frequencies is not present in nature. There are two main approaches to construct a hyperbolic metamaterial. One approach consists in stacking alternating metal-dielectric layers. Each layer has subwavelength dimensions (Figure 2 a)). The second approach consists in metallic nanowires put inside a dielectric host (Figure 2 b)). The selection of the metal-dielectric combination depends in the wavelengths considered. For example, for the ultraviolet regime the combination of Au or Ag as metals and Al_2O_3 as dielectric allows the creation of HMM. In the visible regime, the combination of Au or Ag with TiO_2 generates HMM [9].

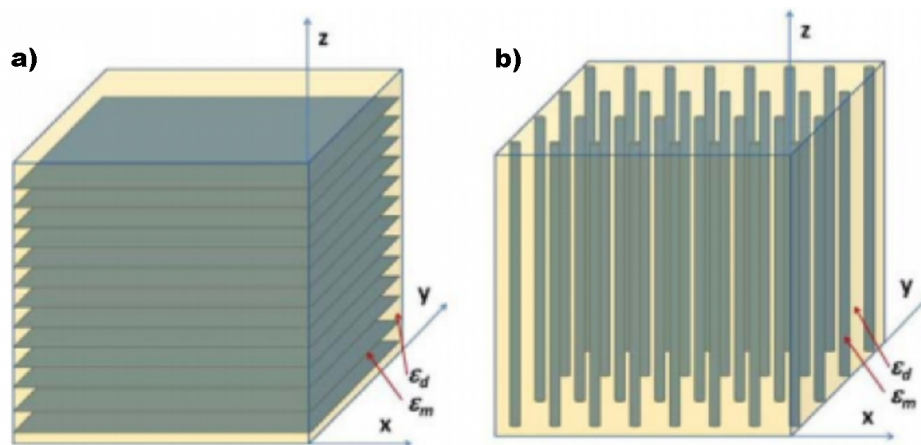


Figure 2: a) HMM made of alternating layers of dielectric and metal. b) HMM made of metallic nanowires inside a dielectric host.

1.3 Aim

The aim of this work is to explain the theoretical development of the differential method for the particular case in which one spatial direction is invariant. Once all the relevant theory behind the method is set, the creation and functioning of a computational tool based on the method is explored. Finally, the analysis of HMMs using the computational tool is considered.

2 Classic differential method

The differential method is a technique used to analyze the diffraction of light due to its interaction with an element of arbitrary shape and made of any periodic or aperiodic arrangement of different materials. The method consists in projecting the electromagnetic field on a set of basic functions in order to obtain a set of ordinary differential equations starting from Maxwell equations [1, 18]. This method is specially suited to treat rough surfaces with localized inhomogeneities (for example air bubbles) and inhomogeneities that are described by changes in the permittivity or in the geometry of the material [12]. In this chapter, a theoretical frame for the method will be developed.

2.1 Definition of the problem

The goal of the method is to compute the electromagnetic field diffracted by a structure. The method will be limited to the particular case in which the structure is invariant along one spacial dimension. Establishing the coordinate axes as in Figure 3, the invariance will be considered along \hat{u}_y .

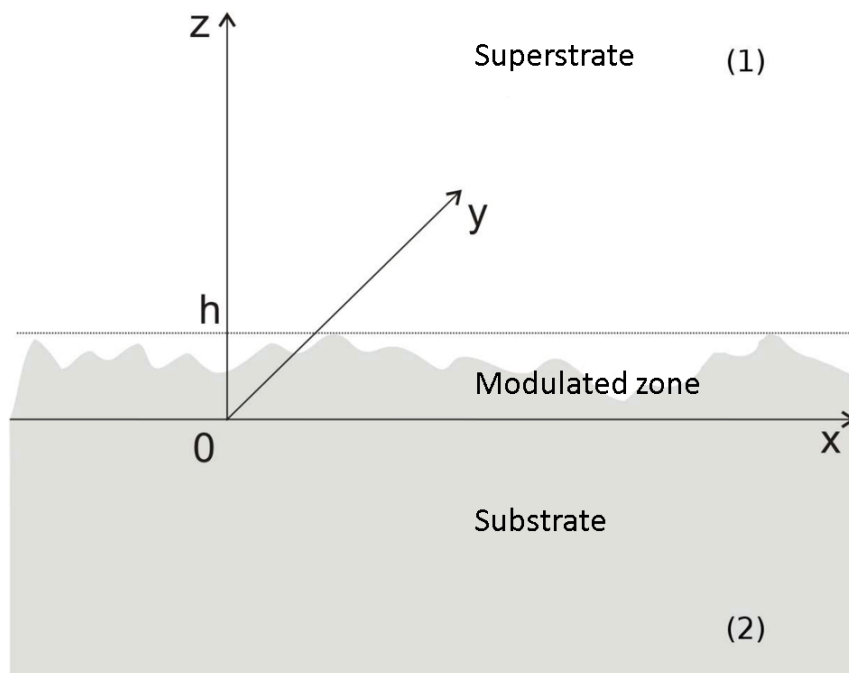


Figure 3: Cartesian coordinate system used to describe a structure invariant along one dimension

The permittivity of the entire system is described as:

$$\begin{aligned}
\epsilon(x, z) &= \epsilon_1 && \text{if } z > h \\
\epsilon(x, z) &= \epsilon(x, z) && \text{if } 0 < z < h \\
\epsilon(x, z) &= \epsilon_2 && \text{if } z < 0
\end{aligned} \tag{1}$$

The region comprised between $0 < z < h$ is called “modulated region”. The zones for $z > h$ and $z < 0$ will be called respectively, superstrate and substrate.

Furthermore, it is going to be assumed that the incident field is a monochromatic plane wave, with wave vector \vec{k} contained in the xz plane and forming an angle θ_i (the angle of incidence) with \hat{u}_y [4]. Finally, the incident wave will be propagating only through the superstrate, there will not be any illumination below the modulated zone (through the substrate).

2.2 Maxwell equations for TE and TM polarizations

The Maxwell equations for a medium in which there is not any currents or charges are:

$$\begin{aligned}
div\vec{D} &= 0 \\
rot\vec{E} &= -\frac{\partial\vec{B}}{\partial t} \\
div\vec{B} &= 0 \\
rot\vec{H} &= \frac{\partial\vec{D}}{\partial t}
\end{aligned} \tag{2}$$

Using a Fourier transform, it is possible to express the time dependence of a vector field $\vec{A}(\vec{r}, t)$ in terms of the angular frequency [18]. Thus, the vector field $\vec{A}(\vec{r}, \omega)$ is such that:

$$\vec{A}(\vec{r}, t) = \int_{-\infty}^{\infty} \vec{A}(\vec{r}, \omega) e^{i\omega t} d\omega \tag{3}$$

Using the Fourier transform as defined in (3) into the set of equations (2), we get:

$$\begin{aligned}
div\vec{D} &= 0 \\
rot\vec{E} &= i\omega\vec{B} \\
div\vec{H} &= 0 \\
rot\vec{H} &= -i\omega\vec{D}
\end{aligned} \tag{4}$$

For a lineal, isotropic and non-magnetic medium we have the relations [13]:

$$\vec{D}(\omega) = \epsilon(\omega)\vec{E}(\omega) \tag{5}$$

$$\vec{B}(\omega) = \mu\vec{H}(\omega) \tag{6}$$

In relation (6) $\mu = \mu_0$ is the magnetic permeability of vacuum.

From (4), by using the equations that involve the rotational operator and combining them with the relations (5) and (6), two different sets of equations are obtained:

$$\begin{aligned} -\frac{\partial E_y}{\partial z} &= i\omega\mu H_x \\ \frac{\partial E_y}{\partial x} &= i\omega\mu H_z \\ \frac{\partial H_x}{\partial z} - \frac{\partial H_z}{\partial x} &= -i\omega\epsilon E_y \end{aligned} \quad (7)$$

$$\begin{aligned} -\frac{\partial H_y}{\partial z} &= -i\omega\epsilon E_x \\ \frac{\partial H_y}{\partial x} &= -i\omega\epsilon E_z \\ \frac{\partial E_x}{\partial z} - \frac{\partial E_z}{\partial x} &= i\omega\mu H_y \end{aligned} \quad (8)$$

These two groups of equations allow us to consider the problem from two different perspectives. Equations (7) represent the transverse electric polarization (TE) or s polarization (the electric field is parallel to the direction \hat{u}_y). On the other hand, the equations (8) describe the transverse magnetic polarization (TM) or p polarization (the magnetic field is parallel to the direction \hat{u}_y) [18].

2.3 Classic differential method for TE polarization

2.3.1 Field equations inside the modulated zone

By applying the rotational operator to the second equation of the set (4) and using the identity $rot(rot\vec{E}) = -\nabla^2\vec{E} + grad(div\vec{E})$, the equation of Helmholtz is obtained:

$$\nabla^2\vec{E} + k^2\vec{E} = \vec{0} \quad (9)$$

Here $k = \mu\epsilon\omega^2 = (2\pi\nu/\lambda)^2$ where $\nu = \sqrt{\epsilon_r\mu_r}$ is the index of refraction of the medium and λ is the free space wavelength of the incident field.

For TE polarization only the component of the electric field parallel to \hat{u}_y is considered. This component is parallel to the surface of the material, thus it is always continuous. After this two considerations, Helmholtz equation becomes:

$$\frac{\partial^2}{\partial z^2}E_y(x, z) = -\frac{\partial^2}{\partial x^2}E_y(x, z) - k^2(x, z)E_y(x, z) \quad (10)$$

E_y can be found solving this equation for $x \in (-\infty, \infty)$ and $z \in [0, h]$. Obviously a complete knowledge of the index of refraction $\nu(x, y)$ in all the modulated zone is necessary.

$$\tilde{A}(\sigma) = \frac{1}{2\pi} \int_{-\infty}^{\infty} A(x)e^{-i\sigma x} dx \quad (11)$$

Using the Fourier transform (11) in equation (10) the dependence on the spatial parameter x is eliminated, obtaining the Helmholtz equation in Fourier space:

$$\frac{\partial^2 \tilde{E}_y}{\partial z^2}(\sigma, z) = \sigma^2 \tilde{E}_y(\sigma, z) - \int_{-\infty}^{\infty} \tilde{k}^2(\sigma - \sigma', z) \tilde{E}_y(\sigma', z) d\sigma' \quad (12)$$

Where \tilde{E}_y and \tilde{k}^2 are the Fourier transform of E_y and k^2 , respectively. The integral is the result of the convolution $(\tilde{k}^2 * \tilde{E}_y)(\sigma, z)$.

In order to solve equation (12) using computational tools, it is necessary to discretize it. This is achieved through the following relations: $\sigma \rightarrow \sigma_n = \sigma_0 + n\Delta\sigma$ and $\sigma' \rightarrow \sigma_m = \sigma_0 + m\Delta\sigma$ for $n, m \in \mathbb{N}$ and $\sigma_0 = k \sin(\theta_i)$, where θ_i is the incidence angle. Also, it is necessary to truncate the equation obtained after the discretization. Thus, it is going to be assumed that the terms of the electric field that corresponds to a spatial frequency greater than certain value σ_N are negligible. The equation obtained after all these considerations is:

$$\frac{\partial^2 \tilde{E}_y}{\partial z^2}(n, z) = \sigma_n^2 \tilde{E}_y(n, z) - \sum_{m=-N}^N \tilde{k}^2(n - m, z) \tilde{E}_y(m, z) \Delta\sigma \quad (13)$$

Where m and n are contained in the interval $[-N, N]$. Using the Kronecker delta and the notation $E_n = \Delta\sigma \tilde{E}_y(n, z)$ y $k_n = \Delta\sigma \tilde{k}^2(n, z)$ this equation can be simplified as:

$$\frac{\partial^2 E_n}{\partial z^2} = \sum_{m=-N}^N [\sigma_n^2 \delta_{n,m} - k_{n-m}^2] E_m \quad (14)$$

This last expression represents a system formed by $(2N + 1)$ differential equations of second order. It can be rewritten as a system of $(4N + 2)$ differential equations of first order:

$$\begin{aligned} \frac{\partial E_n}{\partial z} &= E'_n \\ \frac{\partial E'_n}{\partial z} &= \sum_{m=-N}^N [\sigma_n^2 \delta_{n,m} - k_{n-m}^2] E_m \end{aligned} \quad (15)$$

By using the definitions $H_n = \Delta\sigma \tilde{H}_x(\sigma_n)$ and $H'_n = \omega\mu H_n$, the first equation of (7) becomes $E'_n = -iH'_n$ and the system (15) is:

$$\begin{aligned} \frac{\partial E_n}{\partial z} &= -iH'_n \\ \frac{\partial H'_n}{\partial z} &= i \sum_{m=-N}^N [\sigma_n^2 \delta_{n,m} - k_{n-m}^2] E_m \end{aligned} \quad (16)$$

Now, it is useful to introduce some vector notation to further simplify the system (16). By defining vectors $[E]$ y $[H']$ as follows:

$$[E] = \begin{bmatrix} E_{-N} \\ \vdots \\ E_n \\ \vdots \\ E_N \end{bmatrix} \quad [H'] = \begin{bmatrix} H'_{-N} \\ \vdots \\ H'_n \\ \vdots \\ H'_N \end{bmatrix} \quad (17)$$

And defining the vector:

$$[F] = \begin{bmatrix} [E] \\ [H'] \end{bmatrix} \quad (18)$$

We can express (16) as:

$$\frac{\partial}{\partial z} [F] = M [F] \quad (19)$$

Where M is a matrix such that:

$$M = i \begin{bmatrix} 0 & -Id \\ M_{21} & 0 \end{bmatrix} \quad (20)$$

Id corresponds to the identity matrix and M_{21} is a matrix with components $M_{n,m} = \sigma_n^2 \delta_{n,m} - k_{n-m}^2$.

2.3.2 Field equations outside the modulated zone

For this case, applying a Fourier transform to the Helmholtz equation (9) leads to the equation:

$$\frac{\partial^2 \tilde{\vec{E}}(\sigma, z)}{\partial z^2} + (k^2 - \sigma^2) \tilde{\vec{E}}(\sigma, z) = \vec{0} \quad (21)$$

This second order differential equation has a solution of the form:

$$\tilde{\vec{E}}(\sigma, z) = \tilde{\vec{A}}^-(\sigma) e^{-i\beta z} + \tilde{\vec{A}}^+(\sigma) e^{i\beta z} \quad (22)$$

In (22) $\tilde{\vec{A}}^+(\sigma)$ and $\tilde{\vec{A}}^-(\sigma)$ correspond to the complex amplitudes of progressive and retrograde waves, respectively (i.e. waves propagating along \hat{u}_z and $-\hat{u}_z$ directions). Also, the parameter β is such that $\beta = \sqrt{k^2 - \sigma^2}$.

In the real space, the solution (22) has the form:

$$\vec{E}(x, z) = \int_{-\infty}^{\infty} \left[\tilde{\vec{A}}^-(\sigma) e^{-i(\sigma x - \beta z)} + \tilde{\vec{A}}^+(\sigma) e^{i(\sigma x + \beta z)} \right] d\sigma \quad (23)$$

This integral can be discretized and truncated to obtain:

$$\vec{E}(x, z) = \sum_{n=-N}^{+N} \left[\tilde{A}_n^- e^{-i(\sigma_n x - \beta_n z)} + \tilde{A}_n^+(\sigma) e^{i(\sigma_n x + \beta_n z)} \right] \Delta\sigma \quad (24)$$

Considering only the component along \hat{u}_y of (24) we obtain:

$$\begin{aligned} E_y(x, z) &= \sum_{n=-N}^{+N} \left[A_n^- e^{-i(\sigma_n x - \beta_n z)} + A_n^+(\sigma) e^{i(\sigma_n x + \beta_n z)} \right] \\ &= \sum_{n=-N}^{+N} E_n e^{i\sigma_n x} \end{aligned} \quad (25)$$

Where $E_n = E_n^- + E_n^+$, $A_n^- e^{-i\beta_n z} = E_n^-$ and $A_n^+ e^{+i\beta_n z} = E_n^+$ (also $A_n^- = \Delta\sigma \tilde{A}_n^-(\sigma_n)$ and $A_n^+ = \Delta\sigma \tilde{A}_n^+(\sigma_n)$) for the propagating waves with directions $-\hat{u}_z$ and \hat{u}_z , respectively. Considering the first equation of the set (7), H'_n is:

$$H'_n = i \frac{\partial E_n}{\partial z} = \beta_n A_n^- e^{-i\beta_n z} - \beta_n A_n^+ e^{i\beta_n z} = \beta_n E_n^- - \beta_n E_n^+ \quad (26)$$

The electric field in the superstrate ($z > h$) is indicated by E_n^h and is given by the sum of the incident field E_n^i and the reflected field E_n^{h+} :

$$E_n^h = E_n^i + E_n^{h+} = A_n^i e^{-i\beta_n^h z} + A_n^{h+} e^{i\beta_n^h z} \quad (27)$$

A_n^i and A_n^{h+} are the complex amplitudes of the incident and reflected fields.

In the substrate ($z < 0$) the electric field is given only by the transmitted field. Thus:

$$E_n^0 = E_n^{0-} = A_n^{0-} e^{-i\beta_n^0 z} \quad (28)$$

A_n^{0-} is the complex amplitude of the transmitted field.

Equations (25) and (26) describe downward and upward propagating fields. These fields have a vectorial representation such that:

$$[E^-] = \begin{bmatrix} E_{-N}^- \\ \vdots \\ E_n^- \\ \vdots \\ E_N^- \end{bmatrix} \quad [E^+] = \begin{bmatrix} E_{-N}^+ \\ \vdots \\ E_n^+ \\ \vdots \\ E_N^+ \end{bmatrix} \quad [V] = \begin{bmatrix} [E^-] \\ [E^+] \end{bmatrix} \quad (29)$$

A relation between vectors (17) and (29) can be established through a matrix Ψ such that $[F] = \Psi [V]$. The form of this matrix comes from equations (25) and (26). The matrix Ψ is:

$$\Psi = \begin{bmatrix} Id & Id \\ \Psi_{21} & \Psi_{22} \end{bmatrix} \quad (30)$$

Where Ψ_{21} and Ψ_{22} are:

$$\Psi_{21} = \begin{bmatrix} \ddots & & 0 \\ & \beta_n & \\ 0 & & \ddots \end{bmatrix} \quad \Psi_{22} = \begin{bmatrix} \ddots & & 0 \\ & -\beta_n & \\ 0 & & \ddots \end{bmatrix} \quad (31)$$

2.4 Classic differential method for TM polarization

2.4.1 Field equation

Applying the operator *rot* to the fourth equation of (4) and the relation (5) we obtain the Helmholtz equation for the magnetic field \vec{H} :

$$\nabla^2 \vec{H} + \omega^2 \mu \epsilon \vec{H} = i\omega \text{grad} \epsilon \times \vec{E} \quad (32)$$

For TM polarization equation (32) turns into:

$$\nabla^2 H_y + \omega^2 \mu \epsilon H_y = i\omega \frac{\partial \epsilon}{\partial z} E_x - i\omega \frac{\partial \epsilon}{\partial x} E_z \quad (33)$$

It is possible to use equations (8) to express E_x and E_z as function of $\partial H_y / \partial z$ and $\partial H_y / \partial x$. The resultant equation is:

$$\frac{\partial}{\partial z} \left(\frac{1}{\epsilon} \frac{\partial H_y}{\partial z} \right) = -\frac{\partial}{\partial x} \left(\frac{1}{\epsilon} \frac{\partial H_y}{\partial x} \right) - \omega^2 \mu H_y \quad (34)$$

This differential equation can be transform in a system of two differential equation of first order considering that $E_x = (1/i\omega\epsilon) \partial H_y / \partial z$. The system obtained is:

$$\begin{aligned} \frac{1}{i\omega\mu} \frac{\partial E_x}{\partial z} &= H_y + \frac{\partial}{\partial x} \left(\frac{1}{k^2} \frac{\partial H_y}{\partial x} \right) \\ \frac{\partial H_y}{\partial z} &= -\frac{1}{i\omega\mu} k^2 E_x \end{aligned} \quad (35)$$

When applying the Fourier transform (defined by (11)) to this system, it is necessary to transform the product $k^2 E_x$. The transformation of this product generates a convolution. The problem with this operation is that k^2 is proportional to $\epsilon(x)$ and this value could present discontinuities inside the modulated zone. Furthermore, the discontinuity of $E_x(x)$ depends on the geometry of the analyzed surface. Consequently, to obtain the correct representation in Fourier space of (35) we have to consider these two elements[18].

2.4.2 Definition of the normal and tangential components at the surface for the electric field

In order to consider the effect of the geometry, it is necessary to define the components normal (E_N) and tangential (E_T) to the surface of the electric field. These components are:

$$\begin{aligned} E_N &= -\sin\theta_N E_x + \cos\theta_N E_z \\ E_T &= \cos\theta_N E_x + \sin\theta_N E_z \end{aligned} \quad (36)$$

The angle θ_N and the components E_N and E_T are illustrated in Figure 4.

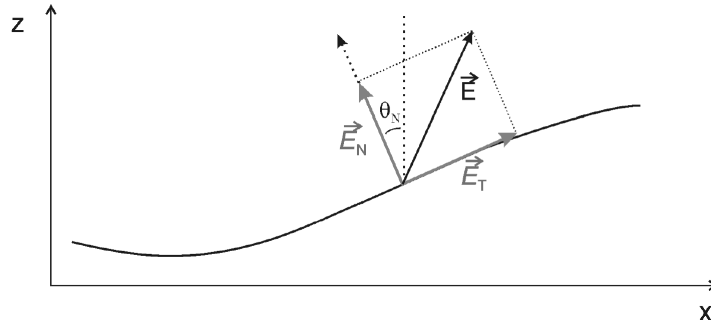


Figure 4: Decomposition of the electric field in normal and tangential components

From equation (4), E_x and E_z can be expressed as functions of the normal and tangential components.

$$\begin{aligned} E_x &= \cos\theta_N E_T - \sin\theta_N E_N \\ E_z &= \sin\theta_N E_T + \cos\theta_N E_N \end{aligned} \quad (37)$$

For simplifying the notation we are going to establish $c = \cos\theta_N$ and $s = \sin\theta_N$.

Assuming that the limit of the modulated zone is described by a continuous function $f(x)$, such that $z = f(x)$, c and s are [18]:

$$c(x, f(x)) = \sqrt{\frac{1}{1 + (\partial f/\partial x)^2}} \quad (38)$$

$$s(x, f(x)) = \sqrt{\frac{1}{1 + (\partial f/\partial x)^2}} \frac{\partial f}{\partial x} \quad (39)$$

Using equations (37), (38) and (39) into (35) allows to avoid the description of the system of equations in terms of E_x .

2.4.3 L. Li factorization rules

As mentioned before, when representing the system (35) in the reciprocal space is necessary to consider the continuity of the factors that are involved in a product that is turned into a convolution [18]. A convolution in Fourier space, after a discretization has the form:

$$h_n = \sum_{-\infty}^{\infty} f_{n-m} g_m \quad (40)$$

(40) is true regardless of the continuity of $f(x)$ or $g(x)$ as long as $n \in [-\infty, \infty]$. Although, when (40) is truncated, the correct expression will depend on the continuity of $f(x)$ y $g(x)$ [22]. Three different cases are analyzed.

- If the functions do not present simultaneous discontinuities, the product can be factorized as:

$$h_n = \sum_{-N}^N f_{n-m} g_m \quad (41)$$

The matrix form of this factorization is $[h] = f [g]$. $[h]$ (or $[g]$) represents a vector with $2N + 1$ components that correspond to the Fourier transform of h (or g). Meanwhile, f is a Toeplitz matrix which elements $f_{n,m}$ are Fourier transforms of f at spatial frequencies such that $(\sigma_n - \sigma_m)$.

- If both functions have a discontinuity simultaneously, but the product $f(x)g(x)$ is continuous in this point. Then, the correct factorization is:

$$h_n = \sum_{-\infty}^{\infty} \left[\frac{1}{f} \right]_{n-m}^{-1} g_m \quad (42)$$

The matrix representation of this factorization is $[h] = 1/f^{-1} [g]$.

- If both functions are discontinuous simultaneously and the product is also discontinuous. Then, it is not possible to factorize the product.

2.4.4 Field equations inside the modulated zone

When obtaining the representation of (35) in the reciprocal space, it is necessary to transform the product $k^2 E_x$. Knowing that $k^2 E_x \propto \epsilon E_x$ we must consider the continuity of ϵ , E_x and the product ϵE_x to apply the appropriate Li's factorization rule. Using (37) for E_x we have:

$$\epsilon E_x = \epsilon c E_T - \epsilon s E_N \quad (43)$$

When changing between interfaces, the function $E_T(x)$ is always continuous. On the other hand, $E_N(x)$ and $\epsilon(x)$ are discontinuous, but the product $\epsilon(x)E_N(x)$ is not (the product corresponds to the electric displacement vector and it is always continuous). In Fourier space, the representation of (43) is:

$$[\epsilon E_x] = [\epsilon c E_T] - [\epsilon s E_N] \quad (44)$$

After the application of the correct Li's factorization rules we obtain:

$$[\epsilon E_x] = \epsilon [c E_T] - \frac{1}{\epsilon} [s E_N] \quad (45)$$

We can replace (36) in (45) and considering $c(x)$ and $s(x)$ as always continuous function:

$$[k^2 E_x] = \left(k^2 c^2 + \frac{1}{k^2} s^2 \right) [E_x] - \left(k^2 - \frac{1}{k^2} \right) cs [E_z] \quad (46)$$

Defining the matrices:

$$Q_1 = \left(k^2 - \frac{1}{k^2} \right) c^2 \quad (47)$$

$$Q_2 = \left(k^2 - \frac{1}{k^2} \right) cs \quad (48)$$

Rewriting (46) as:

$$[k^2 E_x] = \left(Q_1 + \frac{1}{k^2} \right) [E_x] + Q_2 [E_z] \quad (49)$$

In a similar way, it is possible to find an expression for $[k^2 E_z]$. This expression is given by:

$$[k^2 E_z] = Q_2 [E_x] + (k^2 - Q_1) [E_z] \quad (50)$$

From this last equation, we can obtain that:

$$[E_z] = (k^2 - Q_1)^{-1} ([k^2 E_x] - Q_2 [E_x]) \quad (51)$$

Introducing the equality $k^2 E_z = i\omega\mu\partial H_y/\partial x$, we get:

$$[E_z] = (k^2 - Q_1)^{-1} \left(i\omega\mu \left[\frac{\partial H_y}{\partial x} \right] - Q_2 [E_x] \right) = - (k^2 - Q_1)^{-1} (\omega\mu\sigma [H_y] + Q_2 [E_x]) \quad (52)$$

Using (52) in (49) the vector $[k^2 E_x]$ becomes:

$$[k^2 E_x] = \left(Q_1 + \frac{1}{k^2}^{-1} - Q_2 (k^2 - Q_1)^{-1} Q_2 \right) [E_x] - \omega \mu Q_2 (k^2 - Q_1)^{-1} \sigma [H_y] \quad (53)$$

Considering the identity $[(1/k^2) \partial H_y / \partial x] = (1/i\omega\mu) [E_z]$, finally we can obtain the correct representation in Fourier space of the system (35). This new system would be:

$$\begin{aligned} \frac{\partial [E_x]}{\partial z} &= -i\sigma (k^2 - Q_1)^{-1} Q_2 [E_x] + i\omega\mu \left(1 - \sigma (k^2 - Q_1)^{-1} \sigma \right) [H_y] \\ \frac{\partial [H_y]}{\partial z} &= \frac{i}{\omega\mu} \left(Q_1 + \frac{1}{k^2}^{-1} - Q_2 (k^2 - Q_1)^{-1} Q_2 \right) [E_x] - iQ_2 (k^2 - Q_1)^{-1} \sigma [H_y] \end{aligned} \quad (54)$$

It is important to highlight that the system (54) represents a system of the form:

$$\frac{\partial}{\partial z} [F] = M [F] \quad (55)$$

When conserving the notation established in (17) and (18) for TE polarization. But, in contrast with TE polarization, matrix M for TM polarization is more complex. For this cases, the M matrix will be:

$$M = i \begin{bmatrix} M_{11} & M_{12} \\ M_{21} & M_{22} \end{bmatrix} \quad (56)$$

Where:

$$\begin{aligned} M_{11} &= -\sigma (k^2 - Q_1)^{-1} Q_2 \\ M_{12} &= \omega\mu \left(1 - \sigma (k^2 - Q_1)^{-1} \sigma \right) \\ M_{21} &= \frac{1}{\omega\mu} \left(Q_1 + \frac{1}{k^2}^{-1} - Q_2 (k^2 - Q_1)^{-1} Q_2 \right) \\ M_{22} &= -Q_2 (k^2 - Q_1)^{-1} \sigma \end{aligned} \quad (57)$$

2.4.5 Field equations outside the modulated zone

Similar to equation (25) found for TE polarization, for TM polarization, the field $H'_y(x, z)$ outside the modulated zone has the form:

$$\begin{aligned} H'_y(x, z) &= \sum_{n=-N}^N [B_n^- e^{-i\beta_n z} + B_n^+ e^{i\beta_n z}] e^{i\sigma_n x} \\ &= \sum_{n=-N}^N H'_n e^{i\sigma_n x} \end{aligned} \quad (58)$$

In (58) we have $H'_n = H_n'^- + H_n'^+$ and we have used the notation $B_n^- e^{-i\beta_n z} = H_n'^-$ and $B_n^+ e^{+i\beta_n z} = H_n'^+$ (we also have considered $B_n^- = \Delta\sigma \tilde{B}^-(\sigma_n)$ and $B_n^+ = \Delta\sigma \tilde{B}^+(\sigma_n)$).

We can express the component $E_x(x, z)$ as a function of $H'_y(x, z)$ (through (8)), thus:

$$E_x(x, z) = -\frac{i\omega\mu}{k^2} \frac{\partial H_y}{\partial z}(x, z) = -\frac{i}{k^2} \frac{\partial H'_y}{\partial z}(x, z) \quad (59)$$

Thanks to this last relation and remembering that $E_n = \Delta\sigma \tilde{E}_x(\sigma_n)$ and $H'_n = \Delta\sigma \tilde{H}'_y(\sigma_n)$, it is easy to establish:

$$\begin{aligned} E_n &= -\frac{\beta_n}{k^2} B_n^- e^{-i\beta_n z} + \frac{\beta_n}{k^2} B_n^+ e^{i\beta_n z} \\ &= -\frac{\beta_n}{k^2} H_n'^- + \frac{\beta_n}{k^2} H_n'^+ \end{aligned} \quad (60)$$

For $z > h$ (superstrate) the magnetic field is formed by the incident and reflected fields. We are going to represent the magnetic field in the superstrate as $H_n'^h$. The incident field will be note as $H_n'^i$ and the reflected as $H_n'^{h+}$. Then:

$$H_n'^h = H_n'^i + H_n'^{h+} = B_n^i e^{-i\beta_n^h z} + B_n^{h+} e^{i\beta_n^h z} \quad (61)$$

B_n^i and B_n^{h+} are the complex amplitudes of the incident and reflected fields.

For $z < 0$ (substrate) the magnetic field is only formed by the transmitted field. Thus, we are going to note this field as:

$$H_n'^0 = H_n'^{0-} = B_n^{0-} e^{-i\beta_n^0 z} \quad (62)$$

B_n^{0-} is the complex amplitude of the transmitted field. It is important to emphasize that there is not any extra incident field below the surface.

As was done in (29), we can define:

$$[H'^-] = \begin{bmatrix} H'_{-N} \\ \vdots \\ H'_n \\ \vdots \\ H'_N \end{bmatrix} \quad [H'^+] = \begin{bmatrix} H'_{-N} \\ \vdots \\ H'_n \\ \vdots \\ H'_N \end{bmatrix} \quad [V] = \begin{bmatrix} [H'^-] \\ [H'^+] \end{bmatrix} \quad (63)$$

After definition (63) we can find a matrix Ψ such that:

$$[F] = \Psi [V] \quad (64)$$

From (60) the matrix is:

$$\Psi = \begin{bmatrix} Id & Id \\ \Psi_{21} & \Psi_{22} \end{bmatrix} \quad (65)$$

Where Ψ_{21} and Ψ_{22} are:

$$\Psi_{21} = \begin{bmatrix} \ddots & & 0 \\ & -\frac{\beta_n}{k^2} & \\ 0 & & \ddots \end{bmatrix} \quad \Psi_{22} = \begin{bmatrix} \ddots & & 0 \\ & \frac{\beta_n}{k^2} & \\ 0 & & \ddots \end{bmatrix} \quad (66)$$

2.5 Resolution of the systems of equations for TE and TM polarizations

The systems (19) and (55) (systems of first order differential equations for TE and TM polarizations) can be solved using different numeric methods for differential equations of first order. But, there is some details that have to be considered. Equations (27), (28), (61) and (62) describe the electric and magnetic fields for TE and TM polarizations at the borders of the modulated zone. The problem is that the coefficients A_n^{h+} , A_n^{0-} , B_n^{h+} and B_n^{0-} are unknown, thus the initial conditions necessary to solve the systems of equations are also unknown. It is possible to cope with this lack of information thanks to the following consideration.

The form of the systems (19) and (55) suggests the existence of a relation between $[F(0)]$ and $[F(0 + dz)]$. This relation is:

$$\begin{aligned} [F(0 + dz)] &= [F(0)] + M(0) [F(0)] dz \\ &= M'(0) [F(0)] \end{aligned} \quad (67)$$

Where $M'(0) = Id + M(0) dz$. The repeated application of (67) allows to find a matrix P such that:

$$[F(h)] = P [F(0)] \quad (68)$$

Thanks to matrix (30) or (65) we can find a matrix T :

$$[V(h)] = T [V(0)] \quad (69)$$

The matrix $T = \Psi^{-1} P \Psi$ is called transmission matrix. This matrix establishes a relation between the incident and transmitted and reflected fields. For TE polarization, for example, we have that $[E^{0+}] = 0$ (the field propagating in the \hat{u}_z direction evaluated at $z = 0$). Then, the submatrices of T generates the relations:

$$[E^i] = T_{11} [E^{0-}] \quad (70)$$

$$[E^{h+}] = T_{12} [E^{0-}] \quad (71)$$

Therefore, we can define matrices $t = T_{11}^{-1}$ and $r = T_{12}T_{11}^{-1}$ that permit find the reflected and transmitted fields only in terms of the incident field, in other words:

$$[E^{h+}] = r [E^i] \quad (72)$$

$$[E^{0-}] = t [E^i] \quad (73)$$

So, it is necessary to find matrix T , even though the shortage of initial conditions. The way to solve this problem is to chose as initial arbitrary condition a vector $[F(0)]_n$, where the n-esime component of the vector is 1 and the others are zero. After to subject this vector to a repeated application of (67) we can find the n-esime column of P . Finally, having matrix P we can find T . The same process can be followed for TM polarization [18].

3 Development of a computational tool for the implementation of the differential method and validation of the code

In this chapter will be discussed some details worth of examination that emerged during the development of a program for implementing the differential method. The two most important elements to be considered when creating the code were: the implementation of the S -matrix propagation algorithm and the Runge-Kutta method for the solution of a systems of equations. A third element related to Fast Fourier Transforms (FFT) is addressed in Appendix A (this topic is left as an appendix due to its focus in a computational point of view). Moreover, different validation steps and their results for the code created will be analyzed. The results provided by the code were verified to obey the energy conservation principle and compared with the results from Fresnel equations and the transmission matrix method. The code developed and used during this particular work was written in C++ language.

3.1 S -matrix propagation algorithm

In equation (69) the relation between the vector V (vector that contains the Fourier components of the electric and magnetic fields propagating in the directions \hat{u}_z or $-\hat{u}_z$, defined by equations (29) or (63)) at both sides of the modulated zone is established through a transmission matrix T . Although, the use of this kind of matrix generates several numerical problems. Labeling two different interfaces as $q + 1$ and q , also two vectors A_{q+1} and A_q , which represent the electromagnetic field amplitudes at the interfaces; the propagation between both, through a transmission matrix is:

$$A_{q+1} = T_{q+1}A_q \quad (74)$$

The source of the numerical instabilities is that the “propagation” between interfaces involves growing and decreasing terms, due to absorption losses and the presence of evanescent waves. When a real field propagates from q to $q + 1$, it does not grown unless the propagation medium supplies optical gains. The same reasoning applies for the propagation from $q + 1$ to q . However, (74) is asymmetrical. This equation can describe the propagation of a natural decreasing field from q to $q + 1$, but when describing the propagation of the exact same field in the opposite direction, the transmission matrix would present artificially growing terms. When the propagation length is sufficiently large this terms overweight the effect of any other term [1]. The path to circumvent these problems consists in introducing the S -matrix algorithm. This tool permits to give a clearer physical interpretation to the matrix that represents the propagation and also to improve the efficiency in computational cost [20].

In order to introduce the S -matrix algorithm in the execution of the designed program, the structure inside the modulated zone is divided in layers. Between each layer an infinitesimal layer of air is put. This idea is represented schematically in Figure 5.

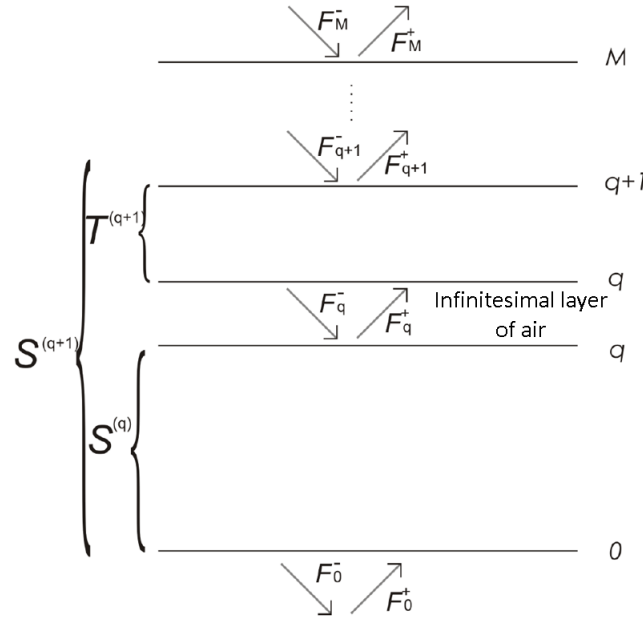


Figure 5: Representation of the division in layers of the modulated zone and definitions of transmission and scattering matrices

As represented in Figure 5 the goal of the program is to establish a matrix S that relates the fields going downward and upward between two interfaces. This matrix is called “scattering” matrix and it generates the relation:

$$\begin{bmatrix} A_q^+ \\ A_0^- \end{bmatrix} = S_q \begin{bmatrix} A_0^+ \\ A_q^- \end{bmatrix} \quad (75)$$

Where A could represent a vector such as E or H' from equations (29) and (63). The matrix can be decomposed in four submatrices:

$$S_q = \begin{bmatrix} S_{11}^{(q)} & S_{12}^{(q)} \\ S_{21}^{(q)} & S_{22}^{(q)} \end{bmatrix} \quad (76)$$

The idea behind the division in layers is to analyze layers short enough such that the transmission matrix does not present numerical instabilities. With this transmission matrix is possible to find the scattering matrix of the layer. Then, the next layer is considered and a transmission matrix is calculated. Finally, a scattering matrix for both layers is obtained in terms of the new transmission matrix and the old scattering

matrix. This process is recursively applied until all the layers were considered. The equations that allow to find a new scattering matrix in terms of previous transmission and scattering matrix (for the submatrices in (76)) are [1]:

$$\begin{aligned}
S_{11}^{(q+1)} &= \left(T_{11}^{(q+1)} - S_{12}^{(q+1)} T_{21}^{(q+1)} \right) S_{11}^{(q)} \\
S_{12}^{(q+1)} &= \left(T_{12}^{(q+1)} + T_{11}^{(q+1)} S_{12}^{(q)} \right) Z_{q+1} \\
S_{21}^{(q+1)} &= S_{21}^{(q)} - S_{22}^{(q+1)} T_{21}^{(q+1)} S_{11}^{(q)} \\
S_{22}^{(q+1)} &= S_{22}^{(q)} Z_{q+1}
\end{aligned} \tag{77}$$

Where:

$$Z_{q+1} = \left(T_{21}^{(q+1)} S_{12}^{(q)} + T_{22}^{(q+1)} \right)^{-1} \tag{78}$$

These submatrices permit to form a matrix such that:

$$\begin{bmatrix} A_{q+1}^+ \\ A_0^- \end{bmatrix} = S_{q+1} \begin{bmatrix} A_0^+ \\ A_{q+1}^- \end{bmatrix} \tag{79}$$

Thus, from (79), a scattering matrix that describes the transmitted (through A_0^-) and reflected (through A_{q+1}^+) fields only in terms of the incident field (the vector A_0^+) can be calculated. Moreover, looking at (75) and (76) a physical interpretation of the submatrices of the scattering matrix can be provided. Considering that for the structure analyzed there is not illumination from below, A_0^+ is a null vector. The submatrices S_{12} and S_{22} are the ones that handle reflection and transmission, respectively. Furthermore, this consideration also permit to avoid the calculation of the complete scattering matrix, reducing the computational cost of this process [18].

3.2 Runge-Kutta method for the solution of a systems of equations

To solve a system of the form:

$$\frac{\partial}{\partial z} [F(z)] = M(z) [F(z)] \tag{80}$$

It is necessary to find a matrix $P(z)$ that relates the vector F at z and $z+h$, in other words:

$$[F(z+h)] = P(z) [F(z)] \tag{81}$$

The matrix $P(z)$ can be find applying a fourth order Runge-Kutta method where the parameter h is the discretization step for the mentioned method. Thus, the matrix is [18]:

$$P(z) = Id + \frac{h}{6}M_1(z) + \frac{h}{3}M_2(z) + \frac{h}{3}M_3(z) + \frac{h}{6}M_4(z) \quad (82)$$

Where:

$$\begin{aligned} M_1(z) &= M(z) \\ M_2(z) &= M\left(z + \frac{h}{2}\right) \left(Id + \frac{1}{2}M_1(z) \right) \\ M_3(z) &= M\left(z + \frac{h}{2}\right) \left(Id + \frac{1}{2}M_2(z) \right) \\ M_4(z) &= M(z+h) (Id + M_1(z)) \end{aligned} \quad (83)$$

The matrix $M_1(z)$ corresponds to either the matrices (20) or (56), depending on the polarization.

For obtaining the scattering matrix for the entire structure, this modified Runge-Kunta method is applied for each layer in which the structure was divided during the S -matrix algorithm. For only one step h of the Runge-Kutta algorithm the end result is the $P(z)$ matrix that allow to fulfill relation (81). A second application of the method will allow to find a matrix P that fulfilled the relation:

$$[F(z+2h)] = P(z+h)[F(z+h)] \quad (84)$$

The appropriate selection of the step h permits to find a unique matrix P that relates the vector $[F(z)]$ and $[F(z+2h)]$. This new matrix is simply the product of $P(z)$ and $P(z+h)$ and the only requirement that need to be satisfied is that h is sufficiently small in order to make both matrix stable [18].

The repeated application of this method until the edge of the considered layer provides a P matrix for all the layer. Once this matrix is obtained, a transmission matrix for the layer can be found as $T = \Psi^{-1}P\Psi$, where Ψ can be either the matrix in (30) or (65).

Finally, once a transmission matrix is obtained for a layer, the S -matrix algorithm can be applied to calculate the scattering matrix of the set of layers considered previously.

The advantages of the application of the Runge-Kutta method as proposed here, not only consist in the fact that it allows to calculate $P(z)$, but also the method reduces the computational resources needed. It allows to avoid the calculation of Ψ , transmission or scattering matrices during the discretization of the structure along the coordinate z . The mayor drawback of this method lays in its dependence on the value of the step h and the necessity to determine it through a process of trial and error. Such problem can be overcome using an adaptative method [17] but the present work does not cover this possibility.

3.3 Code validation

3.3.1 Energy conservation

The first step to validate a code is to verify if it satisfies basic physical principles. One of those principles is the conservation of energy. The reflected and transmitted fields determined by the program must obey the mentioned principle. The first test at which the code was subjected was the calculation of the transmittance and reflectance coefficients for a slab of air and a slab of dielectric material. The two mentioned coefficients were selected to characterize the structure because they are extremely easy to calculate from the scattering matrix [18] and their physical meaning is well known. Calling the reflectance and transmittance coefficients as R and T , respectively; the program must show that $R + T = 1$ for dielectric materials.

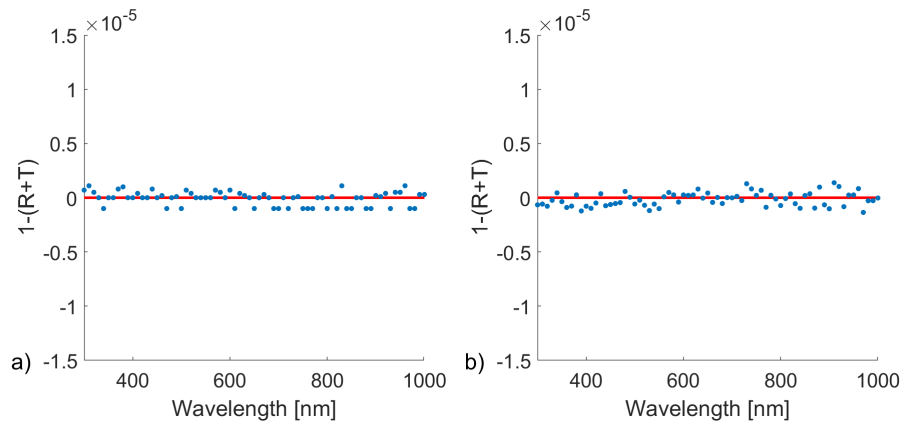


Figure 6: a) Behavior of the reflectance and transmittance coefficients of a slab of air (index of refraction $\nu = 1$) of height 100 [nm], divided in 10 layers and for which 10 Runge-Kunta steps were considered. Angle of incidence $\theta_i = 0$. b) Behavior of the reflectance and transmittance coefficients of a slab of dielectric (index of refraction $\nu = 4$) of height 100 [nm], divided in 10 layers and for which 10 Runge-Kunta steps were considered. Angle of incidence $\theta_i = 0$.

In Figure 6 are shown the behavior of the coefficients as function of the wavelength for a slab of air and a slab of dielectric. Each discrete point correspond to a wavelength between 300 and 1000 [nm] and are separated in steps of 10 [nm]. In both cases the difference between the sum and one is at worst of the order of 1.5×10^{-6} . Thus, there is a very good agreement with the notion of energy conservation. Moreover, for Figure 6, graph a), the mean values of the reflectance is $R = 0.104 \times 10^{-30}$ and of the transmittance is $T = 1.000$. This means that all the energy is transmitted and no energy is reflected, what was expected from a wave propagating in vacuum. In the graph b), the mean values are $R = 0.448$ and $T = 0.552$, the presence of the dielectric material

reduces the transmission of energy and increases the reflection. Finally, in both cases, the polarization TE and TM generates the same results, as spectated from the angle of incidence $\theta_i = 0$.

3.3.2 Comparison with Fresnel equations

In order to figure out if the program can describe correctly the behavior of a metal slab, the results generated by the program are compared with the transmittance and reflectance coefficients obtained from Fresnel equations [28]. The coefficients for a slab of gold (Au) were found using both methods and then compared.

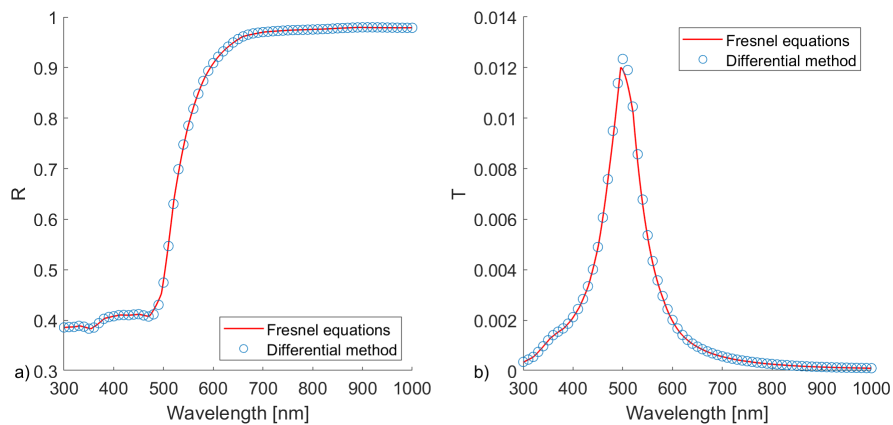


Figure 7: Reflectance and transmittance coefficients of a gold slab of height 100 [nm] divided in 10 layers and for 10 Runge-Kutta steps and an angle of incidence of 0° . a) Reflectance. b) Transmittance.

The coefficients for normal incidence are shown in Figure 7. Once again, the coefficients calculated by the differential method were calculated in an interval of wavelengths from 300 to 1000 [nm], in steps of 10 [nm]. The index of refraction of the metal is wavelength dependent and this information was retrieved from [14]. When comparing the results of both methods, in average, there is a percentage error of 0.151% for the reflectance and 1.974% for the transmittance. Moreover, due to the angle of incidence the TE and TM polarizations are the same.

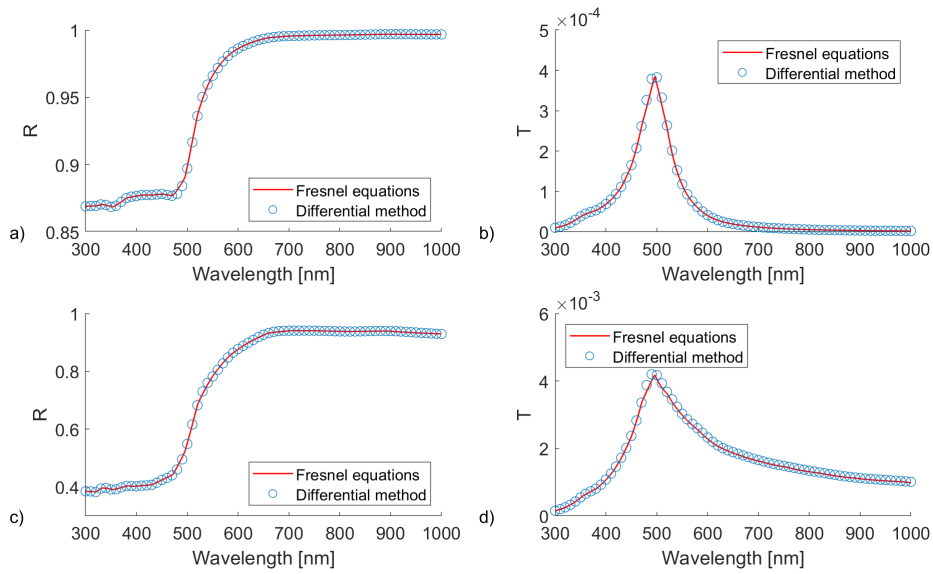


Figure 8: Reflectance and transmittance coefficients of a gold slab of height 100 [nm] divided in 10 layers and 10 Runge-Kunta steps and an angle of incidence of 30° . a) Reflectance for TE polarization. b) Transmittance for TE polarization. c) Reflectance for TM polarization. d) Transmittance for TM polarization.

In Figure 8 are shown the coefficients for the same conditions of Figure 7, but now with a 30° angle of incidence. For this case the two different polarizations generate different results. When comparing the differential method and the Fresnel equations, the average percentage error are presented in Table 1. The value of the errors reflects the good agreement between the two methods.

	TE polarization	TM polarization
Reflectance	0.022%	2.058%
Transmittance	0.160%	1.831%

Table 1: Average percentage error when comparing the differential method and Fresnel equations for a slab of Au of height 100 [nm] divided in 10 layers and 10 Runge-Kutta steps and an angle of incidence of 30° .

It is interesting to mention that both methods for the slab of Au present an increase in reflectance and a peak in transmittance around 500 [nm]. This behavior of the coefficients has an origin of considerable complexity. This effect is a combination of the presence of a surface plasmon resonance and an interband transition where d-electrons are promoted to the s-p conduction band [24].

One major problem with the code developed was found during this stage of the the work. Until this point, the substrate and superstrate were considered as air (index of

refraction $\nu = 1$). When the substrate or the superstrate was changed by a different material (for example, glass or water) the results from the differential method and Fresnel equations were considerably different. The problem arose due to the fact that the program puts an infinitesimal layer of air between each layer in which the structure is divided. Also, one of this infinitesimal layers of air is put between the structure and the substrate or the superstrate. Thus, the program is unable to “see” the substrate or superstrate. The way in which was possible to eliminate this effect was to take advantage of one of the strong points of the differential method, the ease with which more layers can be added to the structure. To simulate the effect of the substrate or superstrate, slabs of finite height are placed above and below the modulated zone. The program considered as its “modulated zone” the combination of the modulated zone and the layers that correspond to the substrate and superstrate. To verify this approach the results were compared with the transmission matrix method.

3.3.3 Comparison with transmission matrix method

This method is a less powerful version of the differential method since it can only describe structures made of different slabs grouped together. The theoretical development of the method is explored in [30]. While, the code used to generate the results of the transmission matrix method is a heavily modified version of [29]. Two different cases were considered. The first one corresponds to a slab of gold surrounded by water (superstrate $\nu = 1.3$ [16]) and glass (substrate $\nu = 1.5$ [16]). The second case consists in a slab surrounded by air (superstrate) and glass (substrate). In both cases, the effect of the substrate and the superstrate is represented by the layers of material above and below the slab of Au. The comparison between both methods is presented in Figure 9.

When comparing the differential method and the transmission matrix method, the average percentage error are presented in Table 2. The value of the errors reflects the good agreement between the two methods. Thus, the option considered is a valid approach to simulate substrates or superstrates made of different materials.

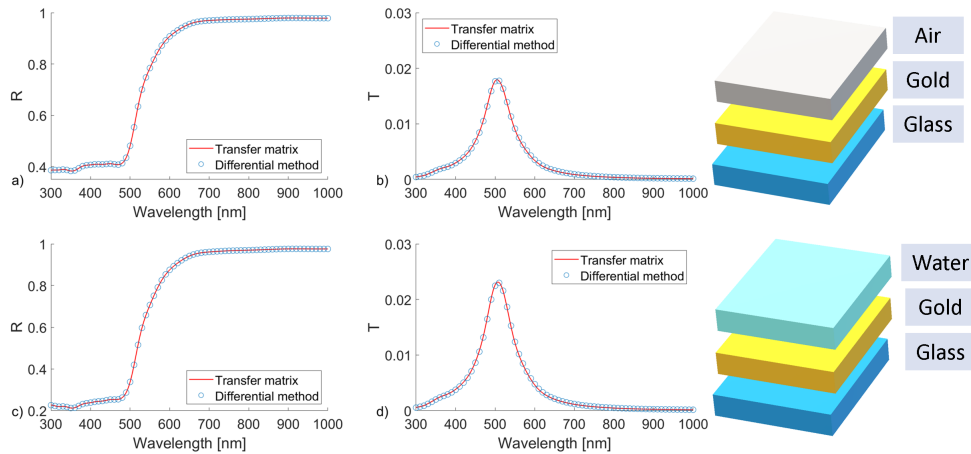


Figure 9: Reflectance and transmittance coefficients of a gold slab of height 100 [nm] divided in 10 layers and for 10 Runge-Kunta steps and an angle of incidence of 0° . a) and b) Reflectance and transmittance when the substrate is made of glass ($\nu = 1.5$, layer of 50 [nm]). c) and d) Reflectance and transmittance when the substrate is made of glass ($\nu = 1.5$, layer of 50 [nm]) and the superstrate is made of water ($\nu = 1.5$, layer of 50 [nm]).

Substrate	Glass	Glass
Superstrate	Air	Water
Reflectance	0.009%	0.031%
Transmittance	4.455%	4.455%

Table 2: Average percentage error when comparing the differential method and transmission matrix method for a slab of Au of height 100 [nm] divided in 10 layers and for 10 Runge-Kunta steps and an angle of incidence of 0° , surrounded by layers that simulate the substrate and superstrate.

4 Applications of the differential method, results and discussion

4.1 Propagation of waves in anisotropic media and hyperbolic meta-materials

4.1.1 Wave propagation

For an anisotropic media, in general, the induced polarization and the electric field are not parallel vectors. The polarization will depend on the magnitude and direction of the electric field:

$$\begin{aligned} P_x &= \epsilon_0 (\chi_{11} E_x + \chi_{12} E_y + \chi_{13} E_z) \\ P_y &= \epsilon_0 (\chi_{21} E_x + \chi_{22} E_y + \chi_{23} E_z) \\ P_z &= \epsilon_0 (\chi_{31} E_x + \chi_{32} E_y + \chi_{33} E_z) \end{aligned} \quad (85)$$

The 3×3 matrix of elements χ_{ij} is called susceptibility tensor. Having into account the relation:

$$\vec{D} = \epsilon_0 \vec{E} + \vec{P} \quad (86)$$

It is possible to establish:

$$\begin{aligned} D_x &= \epsilon_0 (\epsilon_{11} E_x + \epsilon_{12} E_y + \epsilon_{13} E_z) \\ D_y &= \epsilon_0 (\epsilon_{21} E_x + \epsilon_{22} E_y + \epsilon_{23} E_z) \\ D_z &= \epsilon_0 (\epsilon_{31} E_x + \epsilon_{32} E_y + \epsilon_{33} E_z) \end{aligned} \quad (87)$$

Where the elements ϵ_{ij} are:

$$\epsilon_{ij} = (1 + \chi_{ij}) \quad (88)$$

ϵ_{ij} corresponds to the elements of the dielectric tensor. It is possible to select the system of reference such that the dielectric tensor would have the form of a diagonal matrix [39].

$$\epsilon = \begin{bmatrix} \epsilon_x & 0 & 0 \\ 0 & \epsilon_y & 0 \\ 0 & 0 & \epsilon_z \end{bmatrix} \quad (89)$$

For a monochromatic plane wave described by an electric field $\vec{E} \exp \left[i \left(\omega t - \vec{k} \cdot \vec{r} \right) \right]$ and a magnetic field $\vec{H} \exp \left[i \left(\omega t - \vec{k} \cdot \vec{r} \right) \right]$ (where $\vec{k} = \frac{\omega \nu}{c} \hat{s}$, \hat{s} is an unitary vector parallel to the direction of propagation of the wave and ν the index of refraction). Using

Maxwell equations $\vec{k} \times \vec{E} = \omega\mu\vec{H}$ and $\vec{k} \times \vec{H} = -\omega\epsilon\vec{E}$ the following equation can be derived:

$$\vec{k} \times (\vec{k} \times \vec{E}) + \omega^2\mu\epsilon\vec{E} = 0 \quad (90)$$

Using tensor (89) in equation (90) the following system is obtained:

$$\begin{bmatrix} \omega^2\mu\epsilon_0\epsilon_x - k_y^2 - k_z^2 & k_x k_y & k_x k_z \\ k_y k_x & \omega^2\mu\epsilon_0\epsilon_y - k_x^2 - k_z^2 & k_y k_z \\ k_z k_x & k_z k_y & \omega^2\mu\epsilon_0\epsilon_z - k_x^2 - k_y^2 \end{bmatrix} \begin{bmatrix} E_x \\ E_y \\ E_z \end{bmatrix} = 0 \quad (91)$$

To avoid having a zero electric field, the matrix determinant must be zero. This determinant is [39]:

$$\frac{k_x^2}{\nu^2 - \epsilon_x} + \frac{k_y^2}{\nu^2 - \epsilon_y} + \frac{k_z^2}{\nu^2 - \epsilon_z} = \left(\frac{\omega}{c}\right)^2 \quad (92)$$

Equation (92) is known as Fresnel equation. It represents a surface in the three dimensional k -space. This surface is known as normal surface and generally is formed by two shells which have four points in common. The two lines that join these points and go through the origin are known as optic axes. Given a direction of propagation, in most of the cases this direction intersects in two points the normal surface. These two k values correspond to two different phase velocities and polarizations [11, 39].

4.1.2 Propagation in an uniaxial media

In many materials there is only one optical axis. This effect occurs when two of the three components of the tensor (89) are equal. For this case, the elements of the tensor will be noted $\epsilon_x = \epsilon_y = \epsilon_{\perp}$ and $\epsilon_z = \epsilon_{\parallel}$. Also, for this case, the Fresnel equation obtained from the system (91) is [39]:

$$\left(\frac{k_x^2 + k_y^2}{\epsilon_{\parallel}} + \frac{k_z^2}{\epsilon_{\perp}} - \frac{\omega^2}{c^2}\right) \left(\frac{k^2}{\epsilon_{\perp}} - \frac{\omega^2}{c^2}\right) = 0 \quad (93)$$

From Fresnel equation, there is two different values for the wave vector, these values are:

$$k_I^2 = k_0^2\epsilon_{\perp} \quad (94)$$

$$k_{II}^2 = \frac{k_0^2\epsilon_{\perp}\epsilon_{\parallel}}{\epsilon_{\parallel}\cos^2\theta_i + \epsilon_{\perp}\sin^2\theta_i} \quad (95)$$

The parameter θ_i is the angle of incidence and $k_0 = \omega^2\mu_0\epsilon_0$. The value k_I corresponds to an ordinary wave; meanwhile, k_{II} represents an extraordinary wave [11].

4.1.3 Hyperbolic metamaterials

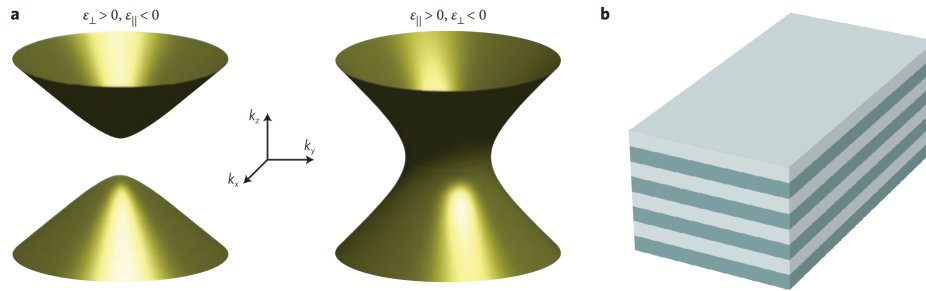


Figure 10: a) Normal surface for an extraordinary wave for a hyperbolic metamaterial. b) Example of a hyperbolic metamaterial made of layers of metal and dielectric materials [25].

It is possible to fabricate materials such that the real parts of ϵ_{\perp} and ϵ_{\parallel} have opposite sign. This material is called a hyperbolic metamaterial (HMM). For HMMs, the normal surface for extraordinary waves (95) takes the form represented in Figure 10 a). The case in which $\epsilon_{\perp} < 0$ and $\epsilon_{\parallel} > 0$ is denominated type I anisotropy. The material behaves as a dielectric in the $x - y$ plane and as a metal in the z direction. For the case $\epsilon_{\perp} > 0$ and $\epsilon_{\parallel} < 0$, the behavior is the opposite and it is called type II anisotropy [5].

The HMMs have different physical properties but one of the most interesting comes from the form of the normal surface in Figure 10 a). The normal surface allows the norm of the k -vector to not be restricted to a finite value. Thus, it is, for example, possible to break the Abbé diffraction limit that establishes that an imaging instrument can not resolve two objects closer than λ/A , where λ is the wavelength of light and A the aperture of the imaging lens [3, 33]. These states which have a non restricted wave vector are called “high k ” states of a hyperbolic metamaterial [9].

One of the possible ways to create a hyperbolic metamaterial is a stack of alternating layers of metal and dielectric materials, as shown in Figure 10 b). The behavior of the components of the dielectric tensor can be studied using effective medium theory provided that the constitutive unitary cell (a single dielectric/metal bilayer) is sub-wavelength [5, 36]. When the losses in the constituent layers can not be neglected the coefficients ϵ_{\parallel} and ϵ_{\perp} are [5]:

$$\epsilon_{\parallel} = \frac{\epsilon'_d t_d + \epsilon'_m t_m + i(\epsilon''_d t_d + \epsilon''_m t_m)}{t_d + t_m} \quad (96)$$

$$\epsilon_{\perp} = \frac{\epsilon'_m t_m D + \epsilon'_d t_d M + i(\epsilon''_m t_m D + \epsilon''_d t_d M)}{(\epsilon'_d t_m + \epsilon'_m t_d)^2 + (\epsilon''_d t_m + \epsilon''_m t_d)^2} (t_d + t_m) \quad (97)$$

In equations (96) and (97) ϵ'_d and ϵ''_d correspond to the real and imaginary parts of the permittivity of the dielectric. Meanwhile, ϵ'_m and ϵ''_m are the real and imaginary parts of the permittivity of the metal. t_d and t_m are the thickness of the layers of dielectric and metal, respectively. Finally, $D = (\epsilon'_d)^2 + (\epsilon''_d)^2$ and $M = (\epsilon'_m)^2 + (\epsilon''_m)^2$.

Using EMT different combinations of metals and dielectrics were studied in order to verify if they present HMM-like properties and how the thickness of the layers affects them. For the arrangement in Figure 10 b), the combination of Au or Ag as metals and TiO_2 or Al_2O_3 causes anisotropies in the spectrum between 300 [nm] and 1000 [nm] [9, 36].

The first system considered was the structure designed and studied in [36]. The metamaterial is made by 8 bilayers of Au (16 [nm] of thickness) and Al_2O_3 (30 [nm] of thickness). The effective permittivities calculated using equations (96) and (97) for this system are shown in Figure 11 (the index of refraction for the Al_2O_3 was obtained from [15]). From the graph, the real parts of ϵ_{\parallel} and ϵ_{\perp} are both positives for $\lambda < 550$ [nm], but for wavelengths $\lambda > 550$ [nm] $\epsilon_{\perp} > 0$ and $\epsilon_{\parallel} < 0$ (anisotropy type II).

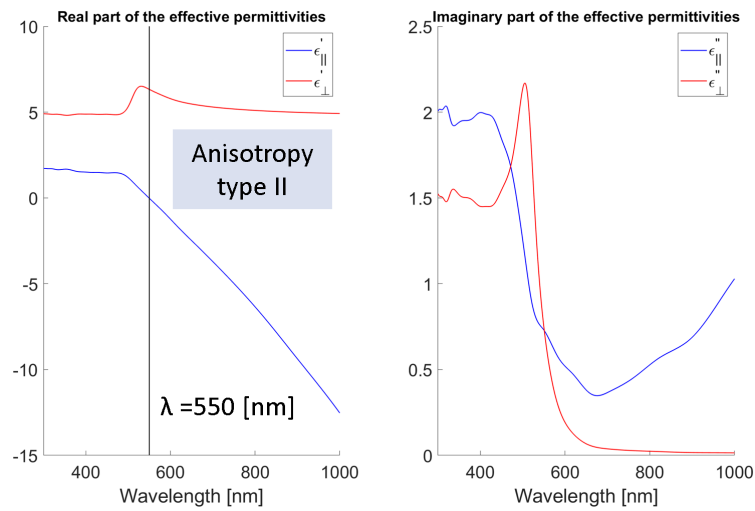


Figure 11: Effective permittivities of a multilayered system made of bilayers of Au (16 [nm] of thickness) and Al_2O_3 (30 [nm] of thickness).

The second system differs from the first one only for the dielectric, that is TiO_2 instead of Al_2O_3 . For this case there is also anisotropy type II for $\lambda > 643$ [nm]. The effective permittivities are shown in Figure 12.

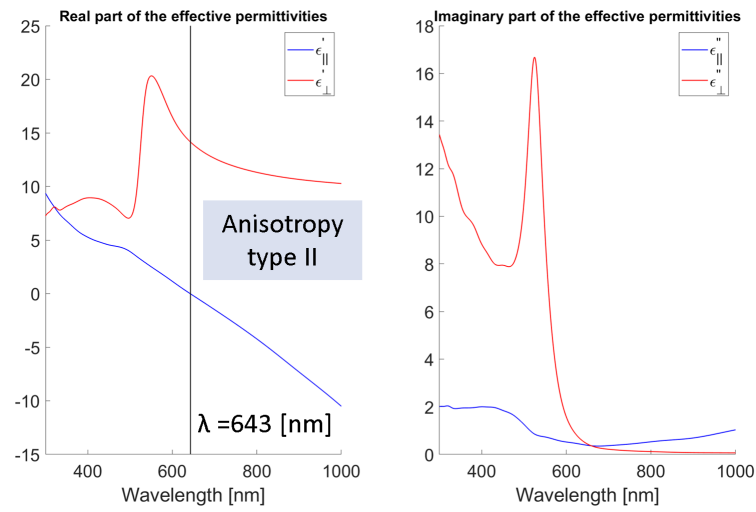


Figure 12: Effective permittivities of a multilayered system mad of bilayers of Au (16 [nm] of thickness) and TiO_2 (30 [nm] of thickness).

For the third system, the metal is changed by Ag and the dielectric is kept as TiO_2 (the information required for the permittivity of the material was retrieved from [10]). Although, for this combination of materials two different thicknesses of bilayers were considered. The first possibility explored was a bilayer of 20 [nm] (with layers of Ag and dielectric of thickness of 10 [nm]). This multilayered system presents two types of anisotropies. For wavelengths > 360 [nm] and < 463 [nm], $\epsilon_{\perp} < 0$ and $\epsilon_{\parallel} > 0$ (type I anisotropy). For wavelengths > 463 [nm], $\epsilon_{\perp} < 0$ and $\epsilon_{\parallel} > 0$ (type II anisotropy). The second case explored was a system of 16 [nm] for Ag and 30 [nm] for TiO_2 . Type I anisotropy is presented for wavelengths > 360 [nm] and < 405 [nm]. Type II anisotropy is presented for wavelengths > 553 [nm].

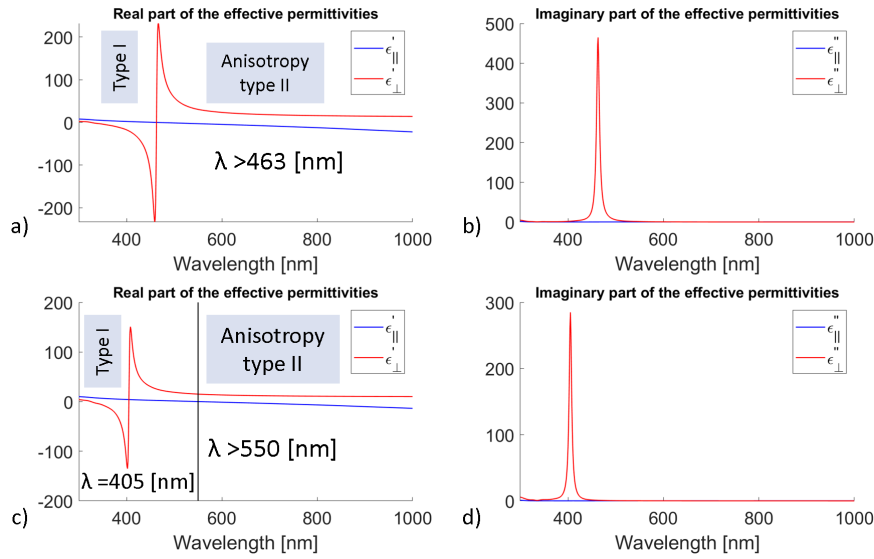


Figure 13: a) and b) effective permittivities of a multilayered system made of bilayers of silver (10 [nm] of thickness) and TiO_2 (10 [nm] of thickness). c) and d) effective permittivities of a multilayered system made of bilayers of silver (16 [nm] of thickness) and TiO_2 (30 [nm] of thickness).

An analysis of the effect of the thicknesses of the metal and the dielectric layers can be derived from the system made of Ag and TiO_2 . Depending on the relation of thicknesses between the metal and the dielectric, the HMM will behave as a pure metal, pure dielectric or will present anisotropies [9]. The behavior of the HMM is represented in Figure 14 and it depends on the filling fraction of metal (the percentage of metal in the HMM). When the metal and dielectric layers have the same thickness (as in Figure 13 a)) the HMM only presents anisotropies. On the other hand, when the dielectric is thicker than the metal (as in Figure 13 c)), there is a regime where the HMM behaves as an effective dielectric (for Figure 13 c) it happens for wavelengths $405 \text{ [nm]} < \lambda < 550 \text{ [nm]}$) and also presents anisotropies outside this regime.

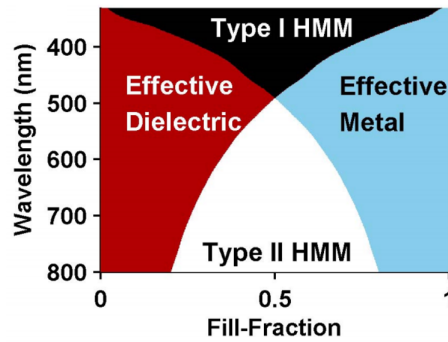


Figure 14: Behavior of a HMM made of Ag and TiO_2 depending on the filling factor of the metal layer

Finally, when comparing Figures 11, 12 and 13 the presence of Au as metal causes that the HMM presents only anisotropies of type II. The effect of changing the dielectric when Au is the metal is analyzed in the next section.

4.2 Analysis of metamaterial using the differential method

In a multilayered system made of several interfaces metal/dielectric surface plasmons polaritons (SPPs) play a fundamental role in the optic response of the metamaterial. But, before the analysis of the metamaterial, it is important to highlight a fundamental fact. SPPs only exist for TM polarization [21]. Thus, from this point, only this polarization will be considered.

However, SPPs are not only resonances that the system shows. The existence of high- k modes allows the system to support volume plasmon polaritons (VPPs) or bulk Bloch plasmon polaritons (BPPs), that are propagating waves inside the material but they decay exponentially outside [34].

In this section the HMMs with metal layers of 16 [nm] and dielectric layers of 30 [nm] will be considered.

For the system of 8 bilayers of Au (16 [nm] of thickness) and Al_2O_3 (30 [nm] of thickness) the reflectance and transmittance spectra are shown in Figure 15. For the case in which the dielectric is replaced by TiO_2 , the reflectance and transmittance are shown in Figure 16.

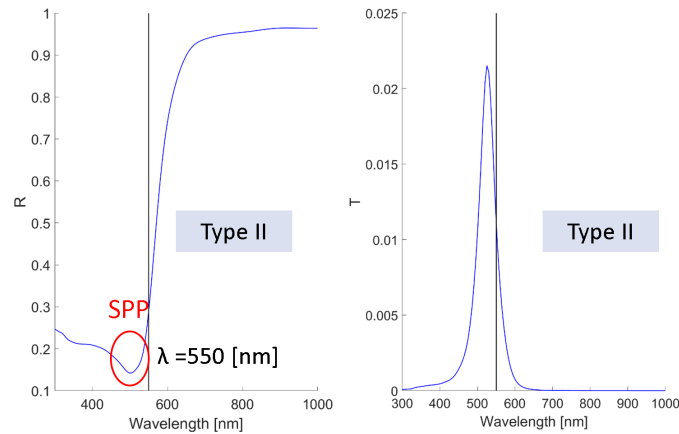


Figure 15: Reflectance and transmittance for a multilayered system of 8 bilayers made of Au (16 [nm]) and Al_2O_3 (30 [nm]), angle of incidence 0° .

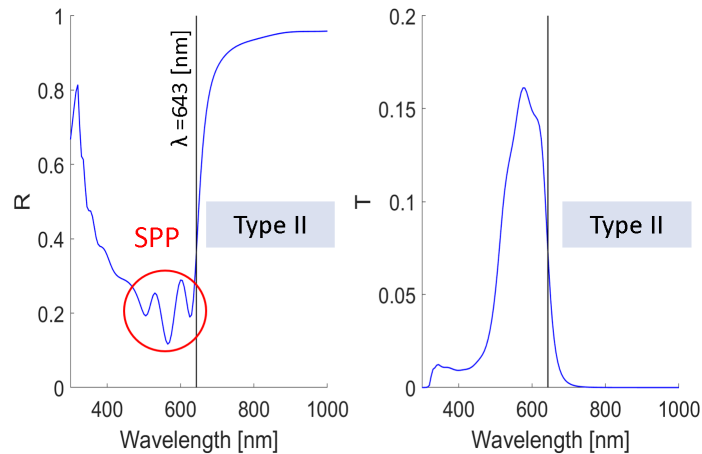


Figure 16: Reflectance and transmittance for a multilayered system of 8 bilayers made of Au (16 [nm]) and TiO_2 (30 [nm]), angle of incidence 0° .

When comparing the spectra in Figure 15 with the one of a slab of metal (for example, the spectra at Figure 7 for a slab of gold of thickness 100 [nm]), the reflectance and transmittance behaves similarly, but the multilayered system presents some interesting details. First, the reflectance in Figure 15 presents a minimum. This minimum appears before the wavelength $\lambda = 550$ [nm]. Thus, it is not due to VPPs (because the minimum appear for wavelengths for which there is not anisotropy) but it is due to SSPs that appears in the interfaces metal/dielectric [35, 34]. Second, the transmittance presents a maximum. The peak in the transmittance also occurs before $\lambda = 550$, then it is not a direct consequence of the anisotropy. However, the fact that the transmittance decays

rapidly after $\lambda = 550$ is due to the anisotropy of type II. Under this regime, the metamaterial behaves as a metal in the z direction and for high wavelengths the transmittance (and also the reflectance) behaves as in Figure 7. The spectra reveal one of the downsides of the metamaterial. The metamaterials presents significant losses, especially for high wavelengths. This losses are mitigated when the peak in transmittance is reached [31]. Finally, it is relevant to mention that the minimum and maximum do not occur for the same wavelength, thus the mode in which the effect of SPPs is relevant does not present the minimum possible losses, at least not for the angle of incidence considered.

On the other hand, Figure 16 also presents minima in the reflectance spectrum caused by SPPs (all the minima happen before $\lambda=643$ [nm] when the metamaterial does not host any anisotropy) and for $\lambda > 643$ [nm] the transmittance decays rapidly. For this case, there are three minima caused by SPPs, this effect is due to the use of TiO_2 as the dielectric. So, it is easier to excite SPPs when using TiO_2 instead of Al_2O_3 .

In Figure 17 are shown the spectra of 8 bilayers of Ag (16 [nm] of thickness) and Al_2O_3 (30 [nm] of thickness).

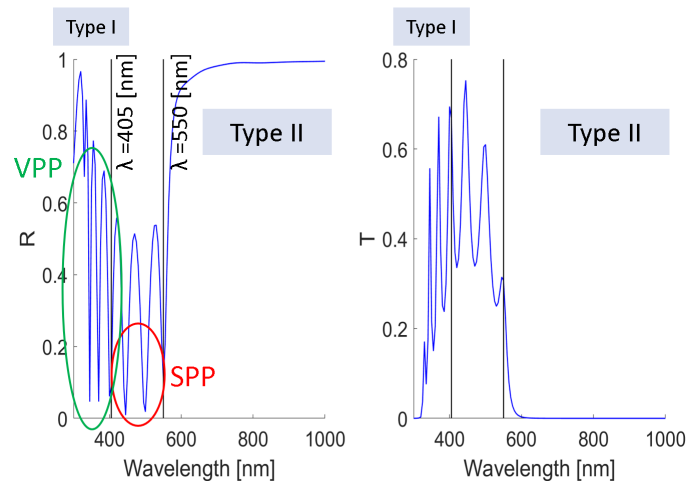


Figure 17: Reflectance and transmittance for a multilayered system of 8 bilayers made of Ag (16 [nm]) and TiO_2 (30 [nm]), angle of incidence 0° .

When changing the metal by Ag, the system does not only present type II anisotropy, but also type I anisotropy. From Figure 17, there are several minima when type I anisotropy appears, meaning that these minima are due to VPPs [36].

From Figures 15, 16 and 17, there is not any minimum when type II anisotropy is present, meaning that there are not VPPs. It is possible to excite VPPs for this regime by using a grating [35]. The combination of the HMM and a grating can be analyzed with the program developed within this work. The HMM that was considered was a multilayered system of 8 bilayers made of Ag (16 [nm]) and TiO_2 (30 [nm]) and the grating is represented in Figure 18. The grating is made of PMMA (the indexes of

refraction as a function of wavelengths were retrieved from [2]) covered by a 20 [nm] layer of Ag. The grating period is 500 [nm].

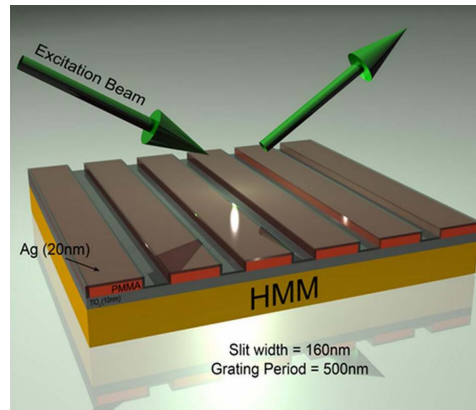


Figure 18: HMM and grating. The HMM is made of 8 bilayers made of Ag (16 [nm]) and TiO_2 (30 [nm]). The HMM and the grating are separated by a layer of 10 [nm] of TiO_2 . The grating is made of PMMA (height of 100 [nm] and length of 160 [nm]) covered by 20 [nm] of Ag. The grating period corresponds to 500 [nm].

The effect of the grating combined with the HMM is shown in Figure 19. As shown by the Figure 19 c), the structure presents a new minimum (that is not present in neither 19 a) nor 19 b)) at $\lambda = 584$ [nm]. This minimum is due to a VPP and occurs when there is type II anisotropy [35, 34].

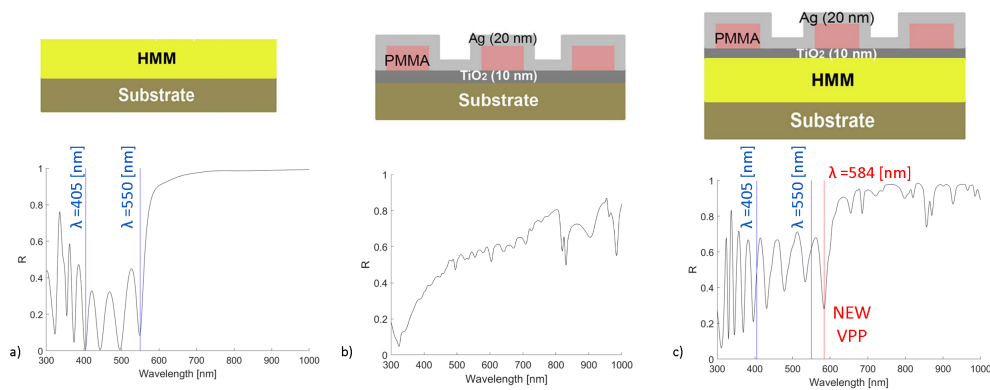


Figure 19: Effect of a grating in a HMM. a) Reflectance of the HMM (8 bilayers of Ag of 16 [nm] and TiO_2 of 30 [nm]). b) Reflectance of the grating of PMMA and Ag. c) Reflectance of the HMM combined with the grating. For all the spectra the angle of incidence was 50° .

5 Conclusions

In this work a code for describing the reflected and transmitted fields based on the differential method was developed. Historically, the biggest problem with the differential method was its inaccuracy to describe the field diffracted by structures for TM polarization. The code created implements elements that eliminate these numerical problems. In this work, it is shown that the use of L. Li factorization rules and S -matrix allow the correct description of the mentioned polarization. The results generated by the code were validated by using the Fresnel equations and the transmission matrix method. When comparing the results obtained by the code and by the other methods, there was a perfect agreement.

After the code validation, it was used to describe HMMs made of alternating layers of metal and dielectric. The study of these structures using the differential method was motivated by the fact that they have been the subject of an intense research activity in the recent years because of their interesting optical properties. The main characteristic of HMMs is that in certain spectral ranges they show permittivities ϵ_{\parallel} and ϵ_{\perp} with real parts of opposite sign; this causes that the HMMs present anisotropies and support “high- k ” modes.

This particular work was focused on the analysis of HMMs made of alternating layers of metal (Au or Ag) and dielectric (Al_2O_3 or TiO_2). In order to verify if this kind of structure presented HMMs-like properties, EMT was used. Once it was confirmed that the structures behaves as HMMs, they were analyzed using the differential method. The reflectance and transmittance spectra of different combinations of materials generated with the code developed confirmed the findings of different research papers used as sources of information for this work. For example, according to the results generated by the code the reflectance spectra of the combination of Au (16 [nm]) and Al_2O_3 (30 [nm]) or Au (16 [nm]) and TiO_2 (30 [nm]) only presented SPPs. While, for the combination of Ag (16 [nm]) and TiO_2 (30 [nm]) VPPs appeared when type I anisotropy occurs and by adding a grating, VPPs occurs also for type II anisotropy. All these behaviors have been studied before and the code developed could reproduce them correctly. Thus the code could be used to simulated novel geometries or combinations of materials in order to kick-start new investigations.

Appendices

Appendix A: Fast Fourier Transform (FFT)

A fundamental element of the differential method is the Fourier transform. Hence, a discussion of how this operation is applied, from a computational point of view, is relevant. Usually, when a numerical procedure for a Fourier transform is considered, a large volume of data is also involved. So, an efficient algorithm is very important.

A Fourier transform of a set of N discrete points is known as discrete Fourier transform (DFT). A straightforward computational algorithm for a DFT only based in the definition of a Fourier transform can result (in the best case scenario) in a computing time proportional to N^2 [23]. But, it is possible to realize this process using a algorithm with a computational time proportional to $N \log_2 N$. This algorithm is called Fast Fourier Transform (FFT). The importance of considering the use of FFTs reside in the enormous difference between the computational times. For example, for $N = 10^6$, choosing the correct algorithm could represent the difference between 30 seconds and two weeks of CPU time on a microsecond cycle time computer [27].

For a function $f(x)$ such that is nonzero for $x \in [0, L]$ and is repeated periodically outside this region, if N discrete points are taken evenly spaced (meaning that the distance between each point is $\Delta x = L/(N - 1)$), then the points of the Fourier transform are separated by intervals of $2\pi/L$. From this information, it is possible to establish that the parameter $\Delta\sigma$ defined in the second chapter is $\Delta\sigma = 2\pi/L$, where L is the length (along \hat{u}_x) of a period of the structure considered [23] [18].

The parameter N fixes the number of discrete points in real and reciprocal spaces, thus the convergence of the method will be strongly dependent on this parameter. But, beyond the suitable magnitude of N necessary to make the method works in different cases, it is possible to establish some general properties of this parameter. First the FFTs are more efficient when the number of discrete points is an even number [27]. Second, the quantity of information that needs to be extracted from the vectors that represent variables in the reciprocal space creates some constraints in the number of discrete points necessary. Considering a particular example allows to illustrate the mentioned constraints. After choosing the discretization parameter N in real space, the value is multiplied by two, to produce an even number. Then, vectors of size $2N$ in Fourier space are produced. But, when looking the size of vectors such that (29), it has size $2N + 1$. Moreover, for a Toeplitz matrix, for example k^2 (appearing in 57), which elements $k_{n,m}^2$ are Fourier transforms of k^2 at spatial frequencies such that $(\sigma_n - \sigma_m)$, of size $2N + 1 \times 2N + 1$, the corners of such a matrix will be equivalent to a Fourier transform at $2N\Delta\sigma$ or $-2N\Delta\sigma$ from the origin. Meaning that the vector that represents the Fourier transform of k^2 would need to have a minimum size of $4N + 1$. There is an obvious lack of information when the discretization in real space is considered for N points, because it generates vectors of size $2N$, when it is necessary vectors of size

$2N + 1$ or $4N + 1$. But, there is some options to overcome this problem.

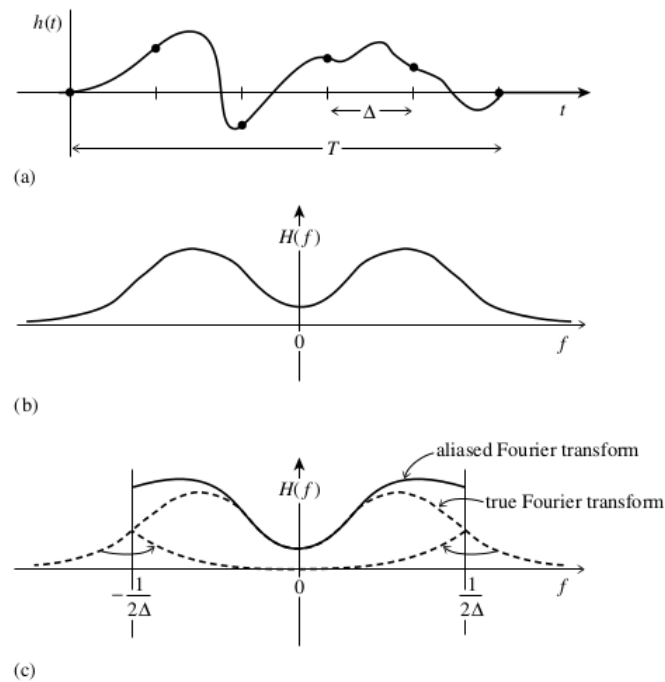


Figure 20: Effect of aliasing in a Fourier transform. a) Function $h(t)$ defined for an interval T (the period of the function) and discretize through intervals of length Δ . b) Fourier transform $H(f)$ of the the function $h(t)$. c) Comparison of the real Fourier transform and the aliased transform inside the region defined by the Nyquist critical frequency $f_c = 1/2\Delta$.

One of the options available is to use a N points Fourier transform (from a N -component vector in real space) and assume that outside the interval defined by these N points, the function in reciprocal spaced behave periodically (as long as it is not too far away from the origin). This possible solution comes from the fact that the Fourier transform of a periodic function is a function well defined inside an interval and zero outside. The inverse is also true. Thus, even though the function in real space is periodic, considering that the function in Fourier space has some degree of periodicity (in order to retrieve the necessary information) is a viable option, but clearly this approach introduces an error. In addition to this error, this option also exacerbates the effect of aliasing. Given a sampling interval in real space as Δ allows to define what is called the Nyquist critical frequency as $f_c = 1/2\Delta$. This parameter is important because it is related to the *sampling theorem*. The theorem states that if a continuous function $h(t)$ with interval sampling Δ is bandwidth limited to frequency smaller than f_c (meaning that $H(f) = 0$ for all $|f| \geq f_c$), then the function $h(t)$ is completely determined by

$h_n = h(n\Delta)$ for n an integer. But, when the function is not bandwidth limited aliasing occurs. All the power spectral density outside $|f| \leq f_c$ is spuriously moved into the range. Aliasing means that the components outside the interval $(-f_c, f_c)$ are falsely transformed [27]. The effect is illustrated in Figure 20. Considering all this observations, this solution is not ideal.

The solution adopted for the code created was, arguably, one of the easiest (effortless to implement in the code) and safest (in the sense that it allows a more precise description in reciprocal space). Instead of sampling the parameters in real space using N points, the discretization is done for $4N$ points (the extra value to obtained vectors of size $4N + 1$ is obtained from the $4N$ points in reciprocal space). The use of a major quantity of points diminishes the negative consequences of the previous solution considered. The biggest problem of this option is the requirement of more computational resources.

6 References

References

- [1] Antonakakis, T. et al. & Popov, E. (Eds.). (2014). *Gratings: Theory and Numeric Applications*. Second Edition. Marseille: Presses Universitaires de Provence.
- [2] Beadie, G., Brindza, M., Flynn, R., Rosenberg, A., & Shirk, J. (2015). Refractive index measurements of poly(methyl methacrylate) (PMMA) from 04–16 μm . *Applied Optics*, 54(31), F139. doi: 10.1364/ao.54.00f139
- [3] Beyond the diffraction limit. (2009). *Nature Photonics*, 3(7), pp.361-361. doi: 10.1038/nphoton.2009.100
- [4] Botten, L. et al. & Petit, R. (Eds.). (1980). *Electromagnetic Theory of Gratings*. New York: Springer.
- [5] Caligiuri, V., Pezzi, L., Veltri, A. and De Luca, A. (2016). Resonant Gain Singularities in 1D and 3D Metal/Dielectric Multilayered Nanostructures. *ACS Nano*, 11(1), pp.1012-1025. doi: 10.1021/acsnano.6b07638
- [6] Canuto, C., Hussaini, M., Quarteroni, A. and Zang, T. (2007). *Spectral methods*. Springer Science & Business Media.
- [7] Cai, W. and Shalaev, V. (2016). *Optical metamaterials*. New York: Springer.
- [8] Cui, T., Smith, D. and Liu, R. (2010). *Metamaterials*. New York: Springer.
- [9] Cortes, C., Newman, W., Molesky, S. and Jacob, Z. (2012). Quantum nanophotonics using hyperbolic metamaterials. *Journal of Optics*, 14(6), p.063001. doi: 10.1088/2040-8978/14/6/063001
- [10] DeVore, J. (1951). Refractive Indices of Rutile and Sphalerite. *Journal of the Optical Society of America*, 41(6), p.416. doi: <https://doi.org/10.1364/JOSA.41.000416>
- [11] Eroglu, A. (2010). *Wave Propagation and Radiation in Gyrotropic and Anisotropic Media*. Indiana University: Springer.
- [12] Giovannini, H., Saillard, M. & Sentenac, A. (1998). Numerical study of scattering from rough inhomogeneous films. *Journal of the Optical Society of America A*, 15(5): 1182-1191.

- [13] Griffiths, D. (2013). *Introduction to Electrodynamics*. Fourth Edition. Boston: Pearson. New York: Marcel Dekker, Inc. doi: <https://doi.org/10.1103/PhysRevB.6.4370>
- [14] Johnson, P. and Christy, R. (1972). Optical Constants of the Noble Metals. *Physical Review B*, 6(12), pp.4370-4379.
- [15] Kelly, R. (1972). Program of the 1972 Annual Meeting of the Optical Society of America. *Journal of the Optical Society of America*, 62(11), p.1336. doi: <https://doi.org/10.1364/JOSA.62.001336>
- [16] Kirkpatrick, L. and Francis, G. (2010). *Physics*. Belmont, CA: Brooks/Cole Cengage Learning.
- [17] Kiusallas, J. (2005). *Numerical Methods in Engineering with Matlab*. Cambridge, Cambridge University Press.
- [18] Laurent, A. (2008). *Diffraktion et diffusion de la lumiere: modelisation tridimensionnelle et application a la metrologie de la microelectronique et aux techniques d'imagerie selective en milieu diffusant*. Atomic Physics. Université Paul Cézanne-Aix-Marseille III.
- [19] Li, L. (1994). Multilayer-coated diffraction gratings: differential method of Chan-dezon et al revisited. *Journal Of The Optical Society Of America A*, 11(11), 2816. doi: [10.1364/josaa.11.002816](https://doi.org/10.1364/josaa.11.002816)
- [20] Li, L. (2003). Note on the S-matrix propagation algorithm. *Journal of the Optical Society of America A*, 20(4), p.655. doi: [10.1364/josaa.20.000655](https://doi.org/10.1364/josaa.20.000655)
- [21] Maier, S. (2007). *Plasmonics*. New York: Springer.
- [22] Neviere, M. & Popov, E. (2002). *Light Propagation in Periodic Media: Differential Theory and Design*
- [23] Pang, T. (2006). *An Introduction to Computational Physics*. Second Edition. Cambridge: Cambridge University Press.
- [24] Patoka, P. and Giersig, M. (2011). Self-assembly of latex particles for the creation of nanostructures with tunable plasmonic properties. *Journal of Materials Chemistry*, 21(42), p.16783. doi: [10.1039/C1JM11936B](https://doi.org/10.1039/C1JM11936B)
- [25] Poddubny, A., Iorsh, I., Belov, P. and Kivshar, Y. (2013). Hyperbolic metamaterials. *Nature Photonics*, 7(12), pp.948-957. doi: [10.1038/nphoton.2013.243](https://doi.org/10.1038/nphoton.2013.243)

- [26] Popov, E., & Nevière, M. (2000). Grating theory: new equations in Fourier space leading to fast converging results for TM polarization. *Journal Of The Optical Society Of America A*, 17(10), 1773. doi: 10.1364/josaa.17.001773
- [27] Press, W., Teukolsky, S., Vetterling, W. and Flannery, B. (1997). *Numerical Recipes in Fortran 77: The Art of Scientific Computing*. Volume 1 of Fortran Numerical Recipes. Second Edition. Cambridge: Cambridge University Press.
- [28] Quimby, R. (2006). *Photonics and Lasers: An Introduction*. New Jersey: John Wiley & Sons, Inc.
- [29] Rao, S. (2016). Transmittance and Reflectance Spectra of Multilayered Dielectric Stack using Transfer Matrix Method. MathWorks. Recover from: <https://la.mathworks.com/matlabcentral/fileexchange/47637-transmittance-and-reflectance-spectra-of-multilayered>
- [30] Rumpf, R. (2011). Improved Formulation of Scattering Matrices for Semi-Analytical Methods that is Consistent with Convention. *Progress In Electromagnetics Research B*, 35, pp.241-261. doi: <http://www.jpier.org/PIERB/pierb35/13.11083107.pdf>
- [31] Savelev, R., Shadrivov, I. and Kivshar, Y. (2015). Wave scattering by metal-dielectric multilayer structures with gain. *JETP Letters*, 100(11), pp.731-736. doi: 10.1134/s002136401423012x
- [32] Smolyaninov, I. and Smolyaninova, V. (2017). Hyperbolic metamaterials: Novel physics and applications. *Solid-State Electronics*, 136, pp.102-112. doi: 10.1016/j.sse.2017.06.022
- [33] Smolyaninov, I. (2018). *Hyperbolic metamaterials*. San Rafael: Morgan & Claypool Publishers.
- [34] Sreekanth, K., De Luca, A. and Strangi, G. (2014). Excitation of volume plasmon polaritons in metal-dielectric metamaterials using 1D and 2D diffraction gratings. *Journal of Optics*, 16(10), p.105103.
- [35] Sreekanth, K., De Luca, A. and Strangi, G. (2013). Experimental demonstration of surface and bulk plasmon polaritons in hypergratings. *Scientific Reports*, 3(1). doi: 10.1038/srep03291
- [36] Sreekanth, K., Alapan, Y., ElKabbash, M., Ilker, E., Hinczewski, M., Gurkan, U., De Luca, A. and Strangi, G. (2016). Extreme sensitivity biosensing platform based on hyperbolic metamaterials. *Nature Materials*, 15(6), pp.621-627. doi: DOI:10.1038/NMAT4609

- [37] Thakur, V. and Chaudhary, D. (2014). Metamaterials: A Leading Edge of Science and Technology. *International Journal of Computer Applications*, 98(9), pp.29-34.
Recover from:
- [38] Tilley, R. (2011). *Colour and the optical properties of materials*. Hoboken, N.J.: Wiley.
- [39] Yariv, A. and Yeh, P. (1984). *Optical Waves in Crystals. Propagation and Control of Laser Radiation*. New York: Wiley & Sons.